Structural bioinformatics

Supplement for "Human structural proteome-wide characterization of Cyclosporine A targets"

Gang Hu[#1], Kui Wang[#1], Jody Groedendyk[#2], Khaled Barakat[3], Marcin J. Mizianty[4], Jishou Ruan[1,5], Marek Michalak[2], Lukasz Kurgan[*4]

[1]School of Mathematical Sciences and LPMC, Nankai University, Tianjin, PR China

[2]Department of Biochemistry, University of Alberta, Edmonton, Alberta, Canada

[3]Faculty of Pharmacy and Pharmaceutical Sciences, University of Alberta, Edmonton, Alberta, Canada

[4]Department of Electrical and Computer Engineering, University of Alberta, Edmonton, Alberta, Canada

[5]State Key Laboratory for Medicinal Chemical Biology, Nankai University, Tianjin, PR China

[#]these authors contributed equally

1 DATA

CSA is a lipophilic, cyclic endacapeptide that weights 1202 Daltons. Previous work has modeled or co-crystallized CSA binding to several proteins including cyclophilins A, B, C, D, E, F, G and H as well as calcineurin; these complexes are available in the Protein Data Bank (PDB) (Berman et al., 2000). We found 91 chains from 30 proteins that include CSA in PDB as of July 2012. The chains with 70 or more inter-atomic contacts (Sobolev et al., 1999) with CSA were kept since this would assure biologically relevant interaction, as shown in (Dessailly et al., 2008); the same criterion was applied in (Hu et al., 2012). Next, we removed redundant chains by filtering them at the 80% sequence similarity using CD-HIT (Li and Godzik, 2006). The resulting 15 protein-CSA complexes that include cyclophilins A, B, C, G, F and a couple of cyclophilin-like folds were used as templates by the ILbind program; they are listed in the Suppl. Table S1.

The structural human proteome was collected from PDB by removing low resolution (< 3Å) structures and, following (Xie, et al., 2007), we kept proteins for which sequences can be mapped to human proteins in Ensembl (Hubbard et al., 2002). Structures of chains with at least 90% sequence identity (measured using BLAST with default parameters) to any human protein from 68th release of Ensembl were selected. We collected total of 9652 human and human-like high resolution protein structures.

2 COMPUTATIONAL MODELING

Putative targets of CSA were selected from the structural human proteome using a three-step process: (1) we predicted each of the targets using ILbind (Hu et al., 2012) and the selected 15 template protein-CSA complexes; (2) we annotated and analyzed putative CSA targets selected based on ILbind scores; and (3) we docked selected subset of putative targets of CSA and advanced them to perform experimental validation; see Suppl. Figure S1.

In the first step, we performed inverse ligand binding predictions with ILbind where the 15 protein-CSA complexes were used to predict other protein targets of CSA and, if appropriate, to approximate position of the site where this interaction occurs. ILbind is a machine learning-based consensus of 15 support vector machines that combines prediction scores generated by two custom-adapted successful, as shown in (Chen et al., 2011), binding site predictors: SMAP (Xie and Bourne, 2008) and FINDSITE (Brylinski and Skolnick, 2008). The inputs to the SVM models, which include alignment length and raw score generated by FINDSITE and SMAP, respectively, were empirically selected from among 14 outputs generated by these two methods. The SVM models were optimized using structures of proteins in complex with three structurally diverse ligands: NAG, ADP, and PLM.

In the second step, top 199 targets with high ILbind scores (> 0.65), which are indicative of a high likelihood to interact with CSA, were subjected to IPA analysis with Ingenuity (www.ingenuity.com). First, protein chains that correspond to PDB structures of the top 199 hits were mapped to UniProt (Consortium, 2012) and the resulting proteins were entered for analysis with Ingenuity. We annotated proteins that are involved in toxicities that are frequently associated with use of CSA, such as cardiotoxicity, hepatotoxicity, and nephrotoxicity. Moreover, we manually scanned PUBMED to find publications that associate the selected protein targets with CSA. The corresponding annotations are given in the Suppl. Table S1.

In the third step we selected three novel CSA targets with relatively high ILbind scores that are involved in apoptotic pathways with links to nephrotoxicity: calpain 2 (CAPN2), caspase 3 (CASP3), and p38 mitogen-activated protein kinase 14 (MAPK14). We performed docking of CSA to each of the three targets and to a set of positive controls. The objective was to validate binding of CSA to the three putative targets, to predict corresponding binding mode and docking energy, and to compare these energies with the energies of the positive controls. Since CSA is flexible, we considered several representative positive controls (proteins in complex with CSA) to sample the conformational space of the bound CSA. The positive controls were chosen by clustering structures of CSA from the 15 template protein-CSA complexes, and choosing one structure for each of the four resulting clusters. The four representative controls include Cyclophilin A (PDBid 3pmp_B), Cyclophilin C (2rmc_A), FAB fragment IGG1-kappa (1ikf_H), and cyclophilin-like protein (2oju_A). We employed molecular dynamics simulations-based methodology to account for flexibility of the CSA and target proteins in the docking. We generated ten CSA conformations and docked them against ten snapshots of structures of each of the three putative targets. Consequently, we carried out three hundred docking simulations to investigate the possible binding modes of CSA to the three targets. For each target, all docking results were ranked by their binding energies and only the top ten hits were retained for further analysis. Each of the top hits was then used as a starting point for an all-atom solvated MD simulation in order to investigate the stability of CSA within the binding pocket of each target and to generate an ensemble for subsequent binding energy analysis.

2.1 Molecular dynamics (MD) simulations

We performed 38 independent MD simulations. This included a long MD simulation (230ns) on a solvated CSA structure to explore its conformational dynamics, 10ns MD simulations on the four CSA-templates complexes (Cyclophilin A, PDBid 3pmp_B; Cyclophilin C, 2rmc_A; FAB fragment IGG1-kappa, 1ikf_H; cyclophilin-like protein, 2oju_A) for binding energy analysis, three 10ns MD simulations on the apo (free) target

protein structures (CAPN2, PDBid 3bow_A; CASP3, 4ehl_A; MAPK14, 3zs5_A) to extract structural ensembles for docking simulations, and finally thirty MD simulations on the top hits as revealed from docking against the three targets. The MD simulations were carried out using the NAMD program (Kale et al., 1999), with the all-hydrogen AMBER99SB force field (Hornak et al., 2006) simulated in a 12Å-wide buffer of water molecules, at a mean temperature of 300K and physiological pH of 7. The CSA parameters were obtained using the generalized amber force field (GAFF) (Wang et al., 2004). Partial charges for the ligand were calculated with the AM1-BCC method using the Antechamber module of AMBER 10. The simulations protocol followed the same procedure as described in previous work (Barakat et al., 2012; 2010; Jordheim et al., 2013). Protonation states of all ionizable residues were calculated using the program PDB2PQR (Dolinski et al., 2007) followed by adding the proper concentrations of sodium and chloride ions to neutralize the systems. Each solvated system was then minimized, heated with heavy restraints on the backbone atoms, equilibrated for 100ps with a gradual removal of the restraints and finally run for production MD simulations with the simulations' lengths as described above. For the CSA-protein complexes, MD simulations were used to generate an ensemble for binding energy calculations by storing the trajectories every 10ps for subsequent binding energy calculations using the MM-PBSA method. The apo MD simulations for the three targets were used to extract representative structures for docking simulations against CSA. For each target apo simulation, snapshots were stored every 1ns to avoid correlation between the different structures for the same target. The stored structures were then processed to remove all water molecules and ions for subsequent docking simulations.

2.2 Clustering analysis

We followed the clustering methodology from (Barakat et al., 2013a; 2012; 2011) to extract the dominant conformations for CSA. The whole 230ns MD trajectory for the CSA solvated peptide was clustered using RMSD conformational clustering by adopting the average-linkage algorithm with cluster counts ranging from 1 to 30 clusters. All C_α-atoms were RMSD fitted to the minimized initial structure in order to remove overall rotation and translation. The clustering quality was quantified by calculating two clustering metrics: the Davies-Bouldin index (DBI) (Davies and Bouldin, 1979) and the SSR/SST "elbow criterion" index (Shao et al., 2007). A high-quality clustering scheme is expected when DBI experiences a local minimum versus the number of clusters used. On the other hand, using the elbow criterion, the percentage of variance explained by the data is expected to plateau for cluster counts exceeding the optimal number of clusters (Shao et al., 2007). Using these metrics, by varying the number of clusters, an adequate clustering is characterized by a local minimum for DBI and a horizontal line for the percentage of variance explained by the data.

2.3 Docking analysis

For each of the three target proteins (CAPN2, CASP3, and MAPK14), ten snapshots were used as rigid targets for docking against the ten dominant CSA conformations, which were extracted from the clustering analysis described in section 1.2. That is, 300 docking simulations were carried out to incorporate the flexibility of the targets and the CSA within docking. All docking runs were performed using version 4.028 of AUTODOCK (Osterberg et al., 2002), by allowing all rotatable bonds to rotate for CAS and keeping the target protein structures as rigid. Each docking box expanded for 72 grid points in each direction with spacing of 0.35Å between every two-adjacent points, enough to cover twice the size of CSA. The setup for the docking runs is based on our previous work (Barakat et al., 2013a; 2012). Using the Lamarckian Genetic Algorithm (LGA), the docking parameters included an initial population of 150 random individuals; a maximum number of 10,000,000 energy evaluations; 100 trials; 30,000 maximum generations; a mutation rate of 0.02; a crossover rate of 0.80 and the requirement that only one individual can survive into the next generation. Only top 10 hits that had the highest affinity for each target were retained for further MD simulations and binding energy analysis.

To validate AUTODOCK, we re-docked the top 10 hits for each target using the induced fit procedure implemented in the molecular operating environment (MOE) software (Molecular Operating Environment, 2003). For each docking simulation, the London dG scoring method was first used to score the docked poses, followed by refinement using the AMBER force field, and then rescoring the refined poses using the GBVI/WSA dG scoring function. The highest scoring pose for each induced fit docking simulation was then compared to the original AUTODOCK docked structure.

2.4 Binding energy analysis

We used the MM-PBSA technique (Kollman et al., 2000) to predict the binding energies. Similar to the work described previously in the literature (Barakat et al., 2013a; 2013b; 2010; Friesen et al., 2012) the total free energy for each system is estimated as the sum of the average molecular mechanical gas-phase energies (E_{MM}), solvation free energies (G_{solv}), and entropy contributions ($-TS_{solute}$) of the binding reaction:

$$G = \mathrm{E_{MM}} + G_{solv} - TS_{solute} \quad \text{(Eq. 1)}$$

The molecular mechanical ($\mathrm{E_{MM}}$) energy of each snapshot was calculated using the SANDER module of AMBER10. The solvation free energy ($\mathrm{G_{solv}}$) was estimated as the sum of electrostatic solvation free energy, calculated by the finite-difference solution of the Poisson–Boltzmann equation in the Adaptive Poisson-Boltzmann Solver (APBS) and non-polar solvation free energy, calculated from the solvent-accessible surface area (SASA) algorithm. For each protein-CSA complex, the binding free energy was approximated by the difference between the bound and free systems:

$$\Delta G^0 = \Delta \mathrm{G_{gas}}^{\text{CSA-protein}} + \Delta \mathrm{G_{solv}}^{\text{CSA-protein}} - (\Delta \mathrm{G_{solv}}^{\text{CSA}} + \Delta \mathrm{G_{solv}}^{\text{protein}}) \quad \text{(Eq. 2)}$$

The parameters used include a dielectric constant for the protein-CSA complex of 1, a dielectric constant for the water of 80, an ionic concentration of 0.15M and a surface tension of 0.005 with a zero surface offset to estimate the nonpolar contribution of the solvation energy.

2.5 Flexibility of CSA and its protein targets

Supplementary Figure S2A shows the root mean square deviations (RMSD) for the 230ns CSA MD simulations. The relatively high fluctuations of the RMSDs suggest that CSA is flexible. The RMSDs fluctuated around 3Å for most of the simulation, with a limited number of conformational transitions, particularly, at the beginning and in the middle of the simulation (see the two inserts in Supplementary Figure S2A). Clustering analysis for the CSA MD simulation is shown in Supplementary Figure S3. Although the SSR/SST graph plateaued for all cluster counts, the DPI index has a local minimum at the ten clusters, suggesting that this is a suitable number of clusters of CSA conformations. Therefore, we extracted ten clusters and their centroids were used as the representative structures for each cluster. The ten selected dominant CSA structures are shown in Supplementary Figure S4. The cyclic nature of the CSA significantly limited the conformational space of the backbone of the peptide. This explains the rapid convergence of the clustering analysis as opposed to what would be expected for noncyclic peptides. The side chains, however, explored their conformational space, particularly, on the outer side of the peptide.

On the other hand, the target and template protein structures are relatively rigid. Structure of CAPN2, for example, showed small fluctuations that were below 0.2Å, indicating a stable/rigid conformation; see Supplementary Figure S2B. The same behavior was observed for the four templates and the other two putative CSA targets (data not shown).

3 EXPERIMENTAL ANALYSIS

The experimental validation concerns the three selected putative targets of CSA: MAPK14, CASP3, and CAPN2; a positive control: cyclophilin A; and a negative control: NF-kappa B p65 (NFKB). NFKB obtained a low ILbind score of 0.58 and is relevant since it exhibits various considered toxicities (see last row in the Suppl. Table S1). Purified proteins were ob-

tained from Abcam (MAPK14, ab95445; CASP3, ab52101; NFKB, ab114150; cyclophilin A, ab86219), and Millipore (CAPN2, 208718). CM5 chips and P20 detergent used in the SPR analysis were from GE, with CSA and all other chemicals from Sigma and of the highest quality available. Enzyme Activity Assay Kits were obtained from Promega (CAPN2, G8501 and CASP3, G8091) and NEB (MAPK14).

3.1 Surface Plasmon Resonance (SPR) technology

The SPR technology is used to validate small molecule binding for drug discovery (Myszka and Rich, 2000; Lofas, 2004; Pattnaik, 2005). SPR is well suited to perform real-time binding analysis and allows for studying interactions in a small volume, sensitive and label-free detection format. Briefly, a target protein is immobilized as the ligand on a solid state biosensor surface. The other molecule, the drug, is injected as the analyte over the ligand, thereby allowing interaction to occur. The SPR biosensor detects changes in molecular weight due to direct binding, reflecting this as Resonance Units (RU). For protein binding, 1 RU is equal to approximately 1 pg/mm2 of binding to the biosensor surface. From these weight changes, based on real-time measurements in the sensorgram, specific kinetics can be calculated including affinity (KD) and association and dissociation rates.

We coupled the three selected putative targets of CSA: MAPK14, CASP3, and CAPN2; a positive control: cyclophilin A; and a negative control: NF-kappa B p65 (NFKB) to standard CM5 chips with the protein diluted in 10 mM sodium acetate, pH 5 at a concentration between 0.5 μM and 1 μM. Total protein coupling ranged between 100 RU and 2500 RU and was optimized for each protein. The running buffer was composed of 10 mM Hepes, pH 7.2, 150 mM NaCl, 1 mM EDTA, 0.005% P20, and 2% ethanol (Wear and Walkinshaw, 2006). The CSA dilution series was carried out using 8000, 4000, 2000, 1000, 500, 250, 125, and 0 nM CSA, with experiments performed in triplicate. We note that clinical use of CSA is usually between 100 nM and 1600 nM (Hauser et al., 1998). CSA was dissolved in 100% ethanol and diluted as needed. Briefly, a CM5 chip was activated using a 1:1 dilution of EDC:NHS as previously described (Martin et al., 2006). Purified protein was diluted to 0.5 or 1 μM in 10 mM NaAc, pH 5 and injected over the activated CM5 chip followed by the blocking solution of 1 M ethanolamine, pH 9. A reference lane with no ligand coupled was also generated to subtract background binding. For each experiment, the signal was corrected against the control surface response to eliminate any refractive index changes due to buffer change. The data were collected at 25 C at a flow rate of 30 μl/min to minimize mass transfer effects. We used the BiaEvaluation 3.0 software (provided with the BiaCore3000 system) to fit the measured data utilizing the 1:1 Langmuir binding model to compute kinetic association and dissociation rate constants and affinity (K_D). Association and dissociation rates and affinity (KD) were calculated for each experiment and averaged. The binding response signals in Resonance Units (RUs) were continuously recorded and presented graphically as a function of time.

3.2 Enzyme activity assays

We further validated the legitimacy of interactions that were analyzed by SPR by showing a direct effect on purified enzyme activity for CAPN2, MAPK14, and CASP3 in the presence of CSA. The enzyme activity assay kits were modified to utilize purified enzyme proteins.

To measure CAPN2 activity in the presence of CSA, we used the Calpain-Glo Protease Assay (Promega), which utilizes a luciferase based substrate (Suc-LLVY-AMC). Briefly, 1 ng/100 μl of purified calpain enzyme samples were prepared on ice in 10 mM Hepes, pH 7.2, followed by the addition of 100 μl of the dilution series of CSA (8000 nM to 0 nM CSA in 10 mM Hepes, pH 7.2). After 30 minutes incubation, 2 mM CaCl2 was added to samples to activate the calpain activity followed by aliquoting in triplicate into plastic tubes for measurement of luciferase activity. 100 μl of the Calpain-Glo reagent containing the substrate Suc-LLVY was added to each tube, followed by 15 minutes incubation. With calpain activity, the substrate is cleaved, allowing luminescence which can be measured in a luminometer (Berthold). Background (no enzyme, no CSA) and positive (no CSA), negative (no enzyme), and vehicle only (2% EtOH) were included. The experiment was performed in triplicate.

As MAPK14 is a kinase enzyme, monitoring of a target phosphorylation substrate can be examined. The MAPK14 activity assay kit (NEB) was modified to be used as an ELISA style assay versus a Western Blot style assay. This was due to the increased sensitivity provided by the ELISA assay, allowing quantification of the kinase activity. This assay measures direct phosphorylation of a substrate protein by detecting the amount of phosphorylation using a phospho-specific antibody, which can then be detected using a secondary antibody tagged with horseradish peroxidase. The amount of horseradish peroxidase can be quantified using a colorimetric assay. Briefly, the wells of an ELISA plate were coated overnight at 4 C with ATF2 recombinant protein provided in the assay kit at a concentration of 1 μg/100 μl diluted in coating buffer (carbonate-bicarbonate, pH 9.6). CSA was prepared as a dilution series (8000 nM to 0 nM) in the kinase buffer (provided in assay kit, 25 mM Tris pH 7.5, 5 mM β-glycerophosphate, 2 mM DTT, 0.1 mM Na_3VO_4, 10 mM $MgCl_2$). Recombinant MAPK14 enzyme was diluted to 0.1 mg/ml in kinase buffer. Diluted MAPK14 was added to each dilution series (30 μl in 300 μl +/- CSA in kinase buffer). Samples were incubated on ice for 30 minutes without the addition of ATP. The ATF2 precoated plate was washed two times with PBS for five minutes, followed by shaking to remove any excess PBS. 100 μl of MAPK14 +/- CSA in kinase buffer were added to each well in triplicate. 200 μM ATP was added to each well to activate the kinase. Negative control (no ATP) and kinase inhibitor control (1 μM staurosporine) were also included. The plate was incubated for 30 minutes at 30 C. Wells were washed five times with PBS-0.25% Tween-20 (PBS-T). 100 ml of PBS-T+2% BSA (PBS-T-BSA) was added to all the wells, followed by 30 minutes incubation at room temperature. Wells were washed once with PBS-T. 100 μl of PBS-T- BSA was added to all wells, followed by 100 μl of a 1:500 dilution of the rabbit anti-phospho-ATF2 Thr71 antibody (provided in assay kit) diluted in PBS-T-BSA. The wells were incubated for 30 minutes at room temperature, and washed with 250 μl of PBS-T, 3 x 5 minutes. 100 μl of the secondary antibody, anti-rabbit horseradish peroxidase conjugated antibody diluted at 1:1000 in PBS-T-BSA was added to all wells. The plate was incubated for 30 minutes at room temperature, followed by 3 x 5 minutes washes with PBS-T. For the color change reaction, 200 μl of OPD (o-phenylenediaminedihydrochloride, Sigma), which reacts with hydrogen peroxide to produce a yellow color, was added. The plate was incubated for 30 minutes followed by measurement in a spectrophotometer set at a wavelength of 492 nm. The experiment was performed in triplicate and included background and positive and negative controls.

To measure CASP3 activity, the Caspase-Glo 3/7 Assay was used (Promega), which utilizes a luciferase based substrate (Ac-DEVD-pNA). Briefly, 1 ng/100 μl of purified CASP3 enzyme samples were prepared on ice in 10 mM Hepes, pH 7.2, followed by the addition of 100 μl of the dilution series of CSA (8000 nM to 0 nM CSA in 10 mM Hepes, pH 7.2). After 30 minutes incubation, samples in triplicate were aliquoted into plastic tubes for measurement of luciferase activity. 100 μl of the Caspase-Glo reagent containing the substrate Ac-DEVD-pNA was added to each tube, followed by 30 minute incubation. With CASP3 activity, this substrate is cleaved, allowing luminescence which can be measured in a luminometer (Berthold). Background (no enzyme, no CSA) and positive (no CSA), negative (no enzyme), as well as with an inhibitor (1 μM z-VAD) controls were included. The experiment was performed in triplicate.

4 EMPIRICAL EVALUATION OF PREDICTIONS

The inverse ligand binding was recently evaluated using relatively small (several hundred proteins) manually curated benchmark datasets (Hu et al., 2012). We perform the first evaluation on the proteomic scale, over ~10000 proteins. We assessed predictive quality of ILbind and other inverse ligand binding predictors using a comprehensive set of experimentally validated (native) CSA targets collected from multiple sources including PDB (tar-

gets that are in complex with CSA), BindingDB (Liu et al., 2007), and DrugBank (Knox et al., 2011). We measure predictive quality using true positive rate: TPR = TP / P; where TP is the count of native CSA targets that were predicted as binding CSA by a given method and P is the count of all native targets. We do not use criteria that rely on the annotation of negatives (proteins that do not bind CSA) since our knowledge of CSA binding partners is limited and thus we cannot assure correctness of the negative annotations. We clustered protein chains in the structural human proteome at 90% and 80% identity using BLASTCLUST and we evaluated the results on the corresponding two sets of clusters, i.e., a given cluster is considered to be a native target of CSA (predicted to bind CSA) if at least one protein in this cluster shares at least 90% (80%) identity with a native target of CSA (at least one protein in this cluster is predicted by bind CSA). The clustering assures that the evaluation is not biased towards targets that are overrepresented with many structures of similar folds. However, this may potentially introduce errors since some of the proteins in a given cluster that includes CSA target(s) in fact may not bind to this compound. This is why we utilize two similarity cutoffs, at 90 and 80% to cluster together only nearly identical chains and chains with high similarity, respectively. In total there are 20 (21 for 80% similarity) clusters out of 4136 (3819 for 80% similarity) clusters that are native targets of CSA based on data from PDB, BindingDB and DrugBank. TPR was measured over a given number of clusters sorted by their predicted scores (using highest score in a given cluster) in the descending order (from the most to the least likely to bind CSA). We computed area under the TPR curve (AUtpr) that is obtained by calculating TPR values between the top ranked cluster and a given *max* fraction of the top ranked clusters and we report values of $AUtpr_{10}$, $AUtpr_{20}$, and $AUtpr_{100}$ for *max* = 10%, 20% and 100% of the top ranked clusters, respectively.

We assessed statistical significance of the difference in predictive performance between ILbind and other considered methods. We selected half of the proteins (clusters) from a given dataset at random ten times and compared the corresponding results with the t-test (given that the measurements are normal) or Wilcoxon test (otherwise). We tested normality with the Anderson-Darling test at the *p*-value of 0.05.

5 DISCUSSION ON CAPN2, CASP3, AND MAPK14 AND THEIR INTERACTIONS WITH CSA

We used inverse ligand binding predictions with ILbind, molecular dynamics and docking, SPR binding analysis, and enzymatic assay measurements to identify and characterize in detail three novel targets of CSA. The use of this drug is intimately associated with the nephrotoxicity, hepatotoxicity and cardiotoxicity. We selected three of our putative targets, calpain 2 (CAPN2), p38 mitogen-activated protein kinase 14 (MAPK14), and caspase 3 (CASP3) for experimental validation using SPR binding assays motivated by their involvement in the abovementioned toxic responses and favorable inverse ligand binding predictions with ILbind and docking results. CAPN2, MAPK14, and CASP3 and have recently been identified to change their activity with CSA treatment, but in all cases the enzyme activity was measured indirectly and it was assumed that these changes occur via another protein and not due to direct binding of CSA (Tornavaca et al., 2011; Chi et al., 2012; Hwang et al., 2012). Our results suggest that toxic side effects of CSA may in fact be mediated by direct binding of CSA to these proteins, which results in changes in their activity. The binding assays of CSA to these three novel targets confirmed our computational results and showed that they are likely to interact. Furthermore, the enzymatic activity assays revealed that CSA directly and substantially affects activity of CAPN2 and MAPK14 (Figure 2A and 2B).

We focused on identifying off-target proteins that participate in the apoptotic response seen with CSA treatment. Our hypothesis was that the apoptosis triggered by CSA may be resulting from CSA binding to apoptotic pathway proteins and enhancing their enzymatic activity, thereby causing the toxic side effects. Therefore, if one was able to block the interaction with the off-target enzyme that was involved in the apoptotic pathway, we could essentially block the toxic side effect.

Calpains are cytosolic, calcium dependent cysteine proteases similar to caspases that are ubiquitously distributed in all animal cells. Unlike caspases, which function only during apoptosis, calpains are also active in normal cellular activities including cell cycle (Choi et al., 1997; Pariat et al., 1997) and cellular remodeling {Potter et al., 1998). They are activated secondary to caspases (Wood and Newcomb, 1999) by the sustained increase in cytosolic calcium levels (Nath et al., 1996). Calpains were observed to influence signal transduction processes by cleaving cytoskeletal proteins, membrane proteins, and enzymes (Saido et al., 1994) and to promote apoptosis and necrosis in renal cells (Smith and Schnellmann, 2012). They are also found to be involved in cell death and cleave several substrates of the apoptotic pathway. Calcium dependent activation of calpains has been implicated in activating caspases with different apoptotic stimuli (Wang, 2000), such as ER stress (Nakagawa and Yuan, 2000), B cell receptor (Ruiz-Vela et al., 1999) and radiation induced apoptosis (Waterhouse et al., 1998). Several other pro-apoptotic proteins, like BAX (Wood et al., 1998; Choi et al., 2001) and Bid (Mandic et al., 2002), are also cleaved by calpain to increase their activity. Calpains may collaborate with caspases in the execution of apoptosis (Wood and Newcomb, 1999). The calpain family is composed of at least six members divided into two groups: tissue specific and ubiquitous. The latter group includes calpains 1 and 2. CAPN2, which we investigated, has been shown to be directly involved in caspase independent apoptosis (Lee and Thevenod, 2008) and was linked to nephrotoxicity (Peyrou et al., 2007). A recent study has determined that kidney androgen regulated protein (KAP) degradation by calpain is involved in kidney disease (Tornavaca et al., 2011). In this study, it was determined that KAP binds cyclophilin B, with the addition of CSA activating CAPN2 in vitro and in vivo. CAPN2 specifically targets KAP for degradation and KAP was suggested to protect against CSA toxicity. As well, KAP expression was decreased in CSA treated mice. Based on our results, we hypothesize that CSA causes nephrotoxicity by directly binding CAPN2, leading to the degradation of KAP.

MAPKs are serine/threonine kinases that, with stimulation, phosphorylate their specific substrates which can lead to either positively or negatively regulated substrates and signaling pathways. Activation of MAPK14 is implicated in inducing apoptosis (Matsuzawa et al., 2002;Wada and Penninger, 2004; Kralova et al., 2008) and this protein has been linked to a number of mechanisms and signaling pathways including protein expression, acetylation, proteolysis and specific phosphorylation of target proteins (Cuadrado and Nebreda, 2010). Some of the molecular targets of MAPK14 are c-Jun (Humar et al., 2007), CHOP (Pomerance et al., 2003), PRAK (New et al., 1998), and p53 (Dong et al., 2012), all involved in cellular apoptosis. Recent work demonstrates that CSA activates MAPK14 pathways leading to downstream cellular apoptosis (Chi et al., 2012), although the direct interaction was not indicated. MAPK14 has been connected to nephrotoxicity and its inhibition was shown to reduce cisplatin induced nephrotoxicity in mice (Ramesh and Reeves, 2005). These reports support our finding that MAPK14 is activated by CSA, which may lead to nephrotoxicity. Furthermore, combined inhibition of MAPK14 and Akt signaling pathways was shown to abolished CSA-mediated pathogenesis of aggressive skin squamous cell carcinomas (Arumugam et al., 2012), possibly pointing to a competitive inhibition of the side effect of CSA dependent activation of MAPK14.

Caspases, a family of cysteine proteases, play a vital role during apoptosis (Demaurex and Distelhorst, 2003; Xu et al., 2005). Activation of caspases triggers a cascade of proteolytic cleavage of specific substrates leading to the activation of nuclease activity, alterations in DNA repair processes and modifications in membrane dynamics (Shi, 2002; Widlak and Garrard, 2005). Effector caspases, such as caspase 3 (which we considered), 6, and 7 are cleaved and activated by an initiator caspase and directly act on cellular components such as the cytoskeleton (Liu et al., 1996; Kluck et al., 1997;

Yang et al., 1997) that subsequently leads to cellular death (Slee et al., 1999). CASP3 triggers cytoskeletal restructuring, followed by fragmentation of the cell into apoptotic bodies by degrading an actin binding protein, gelsolin (Elmore, 2007). Our finding concerning the CSA-CASP3 interaction provides new insights into the CSA induced apoptosis.

CSA has been abundantly identified to be involved in the induction of apoptosis (Kitagaki et al., 1996; McDonald et al., 1996; Thomas and Cook, 1998; Ortiz et al., 1998; Takeda et al., 1998; Justo et al., 2003; Eckstein et al., 2005; Andrikos et al., 2005; Sato et al., 2011; de Arriba et al., 2013). We hypothesize that CSA may be causing apoptosis and therefore possible toxic side effects also by activating the three novel off-target enzymes that we characterized. Interestingly, literature shows that these targets are interconnected with each other, which could possibly amplify effects of CSA. For example, increases in CAPN2 levels lead to activation of CASP3 in a dose dependent manner in neuronal cells (Blomgren et al., 2001), and on the flip side, a reduction in active CASP3 levels can be attributed to the calpain activation (Bizat et al., 2003). Additionally, calpastatin protein, an inhibitor of calpains, decreases activation of CASP3 (Blomgren et al., 2001). Moreover, active CASP3 was shown to degrade calpastatin, triggering further activation of CAPN2 and cellular necrosis (Neumar et al., 2003). A direct link between CASP3 and MAPK14 was observed in human neutrophils (Alvarado-Kristensson et al., 2004) and activation of MAPK14 was found to be necessary for cleavage of CASP3 in neuronal cells in rat (McLaughlin et al., 2001). Activation of MAPK14 was also shown to increase activity of CASP3 in mouse T-lymphocytes (Farley et al., 2006). As well, gene knockout of MAPK14 leads to a decrease in activation of mouse CASP3 under serum starvation conditions (De Chiara et al., 2006).

To sum up, we provide several new insights that shed light on mechanisms that could lead to CSA-induced toxicity based on interactions with the three novel targets. Our results suggests that treatment with specific inhibitors of CAPN2, MAPK14, and CASP3 in combination with CSA may eliminate some of the negative side effects that occur upon CSA mediated activation of these proteins. To this end, a specific CASP3 inhibitor, Ac-DEVD-CHO, was shown to mitigate CSA-induced apoptosis in rat (Grub et al., 2000). Interestingly, calpain inhibitors suppress MAPK14 phosphorylation (Lizama et al., 2009) and MAPK14 is required to stimulate CAPN2 activity (Su et al., 2010).

REFERENCES

Alvarado-Kristensson M, *et al.* (2004) p38-MAPK signals survival by phosphorylation of caspase-8 and caspase-3 in human neutrophils. *J Exper Med* **199**: 449-458.

Andrikos E, et al. (2005) Effect of cyclosporine, mycophenolate mofetil, and their combination with steroids on apoptosis in a human cultured monocytic U937 cell line. *Transplant Proc* **37**: 3226-3229.

Arumugam A, *et al.* (2012) Combined inhibition of p38 and Akt signaling pathways abrogates cyclosporine A-mediated pathogenesis of aggressive skin SCCs. *Biochem Bioph Res Comm* **425**: 177-181.

Barakat KH, *et al.* (2013)A Computational Model for Overcoming Drug Resistance Using Selective Dual-Inhibitors for Aurora Kinase A and Its T217D Variant. *Mol Pharm* **10**: 4572-89.

Barakat KH, *et al.* (2013) Detailed computational study of the active site of the hepatitis C viral RNA polymerase to aid novel drug design. *J Chem Inform Model* **53**, 3031-43.

Barakat KH, *et al.* (2012) Virtual screening and biological evaluation of inhibitors targeting the XPA-ERCC1 interaction. *PloS ONE*, **7**, e51329.

Barakat KH, Tuszynski J (2011) Relaxed complex scheme suggests novel inhibitors for the lyase activity of DNA polymerase beta. *J Mol Graph Model* **29**, 702-16.

Barakat KH, *et al.* (2010). Ensemble-based virtual screening reveals dual-inhibitors for the p53-MDM2/MDMX interactions. *J Mol Graph Model* **28**:555-68.

Berman HM, *et al.* (2000) The Protein Data Bank. *Nucleic Acids Res* **28**, 235-242.

Bizat N, *et al.* (2003) In vivo calpain/caspase cross-talk during 3-nitropropionic acid-induced striatal degeneration - Implication of a calpain-mediated cleavage of active caspase-3. *J Biol Chem* **278**: 43245-43253.

Blomgren K, *et al.* (2001) Synergistic activation of caspase-3 by m-calpain after neonatal hypoxia-ischemia - A mechanism of "pathological apoptosis"? *J Biol Chem* **276**: 10191-10198.

Chi JY, *et al.* (2012) Cyclosporin A induces apoptosis in H9c2 cardiomyoblast cells through calcium-sensing receptor-mediated activation of the ERK MAPK and p38 MAPK pathways. *Mol Cell Biochem* **367**: 227-236.

Choi YH, *et al.* (1997) Regulation of cyclin D1 by calpain protease. *J Biol Chem* **272**: 28479-28484.

Choi WS, Lee EH, Chung CW, Jung YK, Jin BK, et al. (2001) Cleavage of Bax is mediated by caspase-dependent or -independent calpain activation in dopaminergic neuronal cells: protective role of Bcl-2. *J Neurochem* **77**: 1531-1541.

Consortium U (2012) Reorganizing the protein space at the Universal Protein Resource (UniProt). *Nucleic Acids Res* **40**, D71-D75.

Cuadrado A, Nebreda AR (2010) Mechanisms and functions of p38 MAPK signalling. *Biochem J* **429**: 403-417.

Davies DL, Bouldin DW (1979) A cluster separation measure. *IEEE Trans. Pattern Anal. Mach. Intell* **1**, 224.

de Arriba G, *et al.* (2013) Cyclosporine A-induced apoptosis in renal tubular cells is related to oxidative damage and mitochondrial fission. *Toxicol Lett* **218**: 30-38

de Chiara G, *et al.* (2006) Bcl-2 phosphorylation by p38 MAPK - Identification of target sites and biologic consequences. *J Biol Chem* **281**: 21353-21361.

Demaurex N, Distelhorst C (2003) Apoptosis - the calcium connection. *Science* **300**: 65-67.

Dessailly BH, *et al.* (2008) LigASite--a database of biologically relevant binding sites in proteins with known apo-structures. *Nucleic Acids Res* **36**, D667-673.

Dolinsky TJ, *et al.* (2007) PDB2PQR: expanding and upgrading automated preparation of biomolecular structures for molecular simulations. *Nucleic Acids Res* **35**, W522-5.

Dong X, *et al.* (2012) p38-NF-?B-promoted mitochondria-associated apoptosis and G2/M cell cycle arrest in norcantharidin-treated HeLa cells. *J Asian Nat Prod Res* **14**: 1008-1019.

Eckstein LA, *et al.* (2005) Cyclosporin a inhibits calcineurin/nuclear factor of activated T-cells signaling and induces apoptosis in retinoblastoma cells. *Invest Ophthalmol Vis Sci* **46**: 782-790.

Elmore S (2007) Apoptosis: A review of programmed cell death. *Toxicol Pathol* **35**: 495-516.

Farley N, *et al.* (2006) p38 mitogen-activated protein kinase mediates the Fas-induced mitochondrial death pathway in CD8(+) T cells. *Mol and Cell Biol* **26**: 2118-2129.

Friesen DE, *et al.* (2012) Discovery of small molecule inhibitors that interact with gamma-tubulin. *Chem Biol Drug Des*, **79**, 639-52.

Grub S, *et al.* (2000) Mechanisms of cyclosporine A-induced apoptosis in rat hepatocyte primary cultures. *Toxicol Appl Pharm* **163**: 209-220.

Hauser IA, *et al.* (1998) Therapeutic concentrations of cyclosporine A, but not FK506, increase P-glycoprotein expression in endothelial and renal tubule cells. *Kidney Int* **54**: 1139-1149.

Hornak V, *et al.* (2006) Comparison of multiple Amber force fields and development of improved protein backbone parameters. *Proteins* **65**, 712-25.

Hu G, *et al.* (2012) Finding protein targets for small biologically relevant ligands across fold space using inverse ligand binding predictions. *Structure* **20**, 1815-1822.

Hubbard T, *et al.* (2002) The Ensembl genome database project. *Nucleic Acids Res* **30**, 38-41.

Humar M, *et al.* (2007) The mitogen-activated protein kinase p38 regulates activator protein 1 by direct phosphorylation of c-Jun. *Intern J Biochem Cell Biol* **39**: 2278-2288.

Hwang EA, *et al.* (2012) Apoptosis in Endothelial Cells by Cyclosporine. *Transplant Proc* 44: 982-984.

Jordheim LP, *et al.* (2013) Small molecule inhibitors of ERCC1-XPF protein-protein interaction synergize alkylating agents in cancer cells. *Mol Pharmacol* **84**, 12-24.

Justo P, *et al.* (2003) Intracellular mechanisms of cyclosporin A-induced tubular cell apoptosis. *J Am Soc Nephrol* **14**: 3072-3080.

Kalé L, *et al.* (1999) NAMD2: Greater scalability for parallel molecular dynamics. *J Comp Phys* **151**, 283-312.

Kitagaki K, *et al.* (1996) Augmentation of apoptosis in bronchial exuded rat eosinophils by cyclosporin A. *Biochem Biophys Res Commun* **222**: 71-77.

Kluck RM, *et al.* (1997) The release of cytochrome c from mitochondria: A primary site for Bcl-2 regulation of apoptosis. *Science* **275**: 1132-1136.

Knox C, *et al.* (2011) DrugBank 3.0: a comprehensive resource for 'omics' research on drugs. *Nucleic Acids Res* **39**:D1035-41.

Kollman PA, *et al.* (2000) Calculating structures and free energies of complex molecules: combining molecular mechanics and continuum models. *Acc Chem Res* **33**, 889-97.

Kralova J, *et al.* (2008) p38 MAPK plays an essential role in apoptosis induced by photoactivation of a novel ethylene glycol porphyrin derivative. *Oncogene* **27**: 3010-3020.

Lee WK, Thevenod F (2008) Novel roles for ceramides, calpains and caspases in kidney proximal tubule cell apoptosis: Lessons from in vitro cadmium toxicity studies. *Biochem Pharma* **76**: 1323-1332.

Li WZ, Godzik A (2006) Cd-hit: a fast program for clustering and comparing large sets of protein or nucleotide sequences. *Bioinformatics* **22**, 1658-1659.

Liu T, *et al.* (2007) BindingDB: a web-accessible database of experimentally determined protein-ligand binding affinities. *Nucleic Acids Res* **35**:D198-201.

Liu XS, *et al.* (1996) Induction of apoptotic program in cell-free extracts: Requirement for dATP and cytochrome c. *Cell* **86**: 147-157.

Lizama C, *et al.* (2009) Calpain Inhibitors Prevent p38 MAPK Activation and Germ Cell Apoptosis After Heat Stress in Pubertal Rat Testes. *J Cell Phys* **221**: 296-305

Lofas S (2004) Optimizing the hit-to-lead process using SPR analysis. *Assay Drug Devel Tech* **2**: 407-415.

Mandic A, *et al.* (2002) Calpain-mediated bid cleavage and calpain-independent Bak modulation: Two separate pathways in cisplatin-induced apoptosis. *Mol Cell Biol* **22**: 3003-3013.

Martin V, *et al.* (2006) Identification by mutational analysis of amino acid residues essential in the chaperone function of calreticulin. *J Biol Chem* **281**: 2338-2346.

Matsuzawa A, *et al.* (2002) Physiological roles of ASK1-mediated signal transduction in oxidative stress- and endoplasmic reticulum stress-induced apoptosis: Advanced findings from ASK1 knockout mice. *Antiox Redox Sign* **4**: 415-425.

McDonald JW, *et al.* (1996) Cyclosporine induces neuronal apoptosis and selective oligodendrocyte death in cortical cultures. *Ann Neurol* **40**: 750-758.

McLaughlin B, *et al.* (2001) p38 Activation is required upstream of potassium current enhancement and caspase cleavage in thiol oxidant-induced neuronal apoptosis. *J Neurosc* **21**: 3303-3311.

Molecular Operating Environment (2013) Chemical Computing Group Inc. http://www.chemcomp/com, 2013.

Myszka DG, Rich RL (2000) Implementing surface plasmon resonance biosensors in drug discovery. *Pharm Sci Technolo Today* **3**: 310-317.

Nakagawa T, Yuan JY (2000) Cross-talk between two cysteine protease families: Activation of caspase-12 by calpain in apoptosis. *J Cell Biol* **150**: 887-894.

Nath R, *et al.* (1996) Effects of ICE-like protease and calpain inhibitors on neuronal apoptosis. *Neuroreport* **8**: 249-255.

Neumar RW, *et al.* (2003) Cross-talk between calpain and caspase proteolytic systems during neuronal apoptosis. *J Biol Chem* **278**: 14162-14167.

New L, *et al.* (1998) PRAK, a novel protein kinase regulated by the p38 MAP kinase. *Embo J* **17**: 3372-3384.

Osterberg F, *et al.* (2002) Automated docking to multiple target structures: incorporation of protein mobility and structural water heterogeneity in AutoDock. *Proteins*, **46**, 34-40.

Ortiz A, *et al.* (1998) Cyclosporine A induces apoptosis in murine tubular epithelial cells: role of caspases. *Kidney Int Suppl* **68**: S25-29.

Pariat M, *et al.* (1997) Proteolysis by calpains: A possible contribution to degradation of p53. *Mol Cell Biol* **17**: 2806-2815.

Pattnaik P (2005) Surface plasmon resonance - Applications in understanding receptor-ligand interaction. *App Biochem Biotech* **126**: 79-92.

Peyrou M, *et al.* (2007) Calpain inhibition but not reticulum endoplasmic stress preconditioning protects rat kidneys from p-aminophenol toxicity. *Toxicol Sci* **99**: 338-345.

Pomerance M, *et al.* (2003) CCAAT/enhancer-binding protein-homologous protein expression and transcriptional activity are regulated by 3 ',5 '-cyclic adenosine monophosphate in thyroid cells. *Mol Endocrin* **17**: 2283-2294.

Potter DA, *et al.* (1998) Calpain regulates actin remodeling during cell spreading. *J Cell Biol* **141**: 647-662.

Ramesh G, Reeves WB (2005) p38 MAP kinase inhibition ameliorates cisplatin nephrotoxicity in mice. *Am J Phys-Renal Phys* **289**: F166-F174.

Ruiz-Vela A, *et al.* (1999) Implication of calpain in caspase activation during B cell clonal deletion. *Embo J* **18**: 4988-4998.

Saido TC, *et al.* (1994) Distinct Kinetics of Subunit Autolysis in Mammalian M-Calpain Activation. *Febs Letters* **346**: 263-267.

Sato M, *et al.* (2011) Cyclosporine A induces apoptosis of human lung adenocarcinoma cells via caspase-dependent pathway. *Anticancer Res* **31**: 2129-2134.

Shao J, *et al.* (2007) Clustering molecular dynamics trajectories: 1. Characterizing the performance of different clustering algorithms. *J Chem Theory Comp*, 2312.

Shi YG (2002) Mechanisms of caspase activation and inhibition during apoptosis. *Mol Cell* **9**: 459-470.

Slee EA, *et al.* (1999) Serial killers: ordering caspase activation events in apoptosis. *Cell Death Differen* **6**: 1067-1074.

Smith MA, Schnellmann RG (2012) Calpains, mitochondria, and apoptosis. *Cardiovasc Res* **96**: 32-37.

Sobolev V, *et al.* (1999) Automated analysis of interatomic contacts in proteins. *Bioinformatics* **15**, 327-332.

Su LT, *et al.* (2010) TRPM7 Activates m-Calpain by Stress-Dependent Stimulation of p38 MAPK and c-Jun N-Terminal Kinase. *J Mol Biol* **396**: 858-869.

Takeda M, *et al.* (1998) Cyclosporine induces apoptosis of mouse terminal proximal straight tubule cells. *Nephron* **80**: 121-122.

Thomas MD, Cook LJ (1998) Fever associated with cyclosporin for treating atopic dermatitis. *BMJ* **317**: 1291.

Tornavaca O, *et al.* (2011) KAP degradation by Calpain is associated with CK2 phosphorylation and provides a novel mechanism for Cyclosporine A-induced proximal tubule injury. *Plos One* **6**(**9**): e25746.

Wada T, Penninger JM (2004) Mitogen-activated protein kinases in apoptosis regulation. *Oncogene* **23**: 2838-2849.

Wang KKW (2000) Calpain and caspase: can you tell the difference? *Trends in Neurosci* **23**: 20-26.

Wang J, *et al.* (2004) Development and testing of a general amber force field. *J Comput Chem*, **25**, 1157-74.

Waterhouse NJ, *et al.* (1998) Calpain activation is upstream of caspases in radiation-induced apoptosis. *Cell Death and Different* **5**: 1051-1061.

Wear MA, Walkinshaw MD (2006) Thermodynamics of the cyclophilin-A/cyclosporin-A interaction: A direct comparison of parameters determined by surface plasmon resonance using Biacore T100 and isothermal titration calorimetry. *Anal Biochem* **359**: 285-287.

Widlak P, Garrard WT (2005) Discovery, regulation, and action of the major apoptotic nucleases DFF40/CAD and endonuclease G. *J Cell Biochem* **94**: 1078-1087.

Wood DE, *et al.* (1998) Bax cleavage is mediated by calpain during drug-induced apoptosis. *Oncogene* **17**: 1069-1078.

Wood DE, Newcomb EW (1999) Caspase-dependent activation of calpain during drug-induced apoptosis. *J Biol Chem* **274**: 8309-8315.

Xie L, *et al.* (2007) In silico elucidation of the molecular mechanism defining the adverse effect of selective estrogen receptor modulators. *Plos Comp Biol* **3**, 2324-2332.

Xu CY, *et al.* (2005) Endoplasmic reticulum stress: cell life and death decisions. *J Clin Invest* **115**: 2656-2664.

Yang J, *et al.* (1997) Prevention of apoptosis by Bcl-2: Release of cytochrome c from mitochondria blocked. *Science* **275**: 1129-1132.

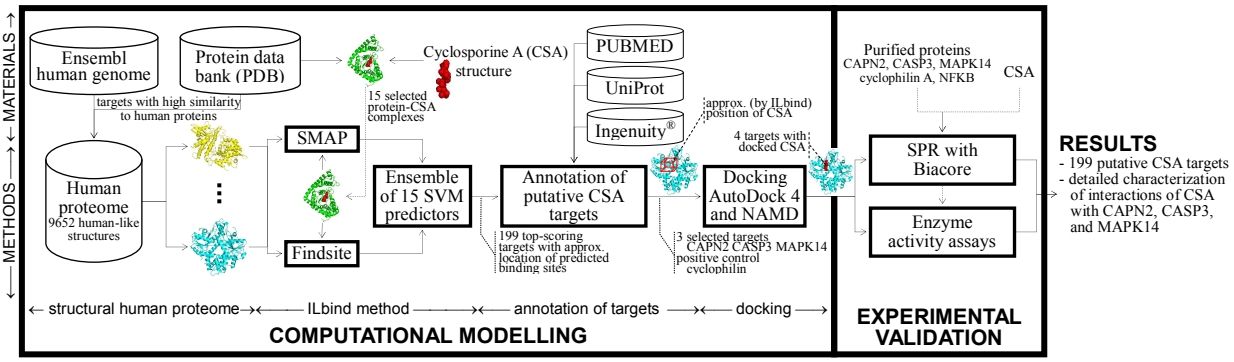

Figure S1. Overview of the pipeline used to predict and characterize CSA targets.

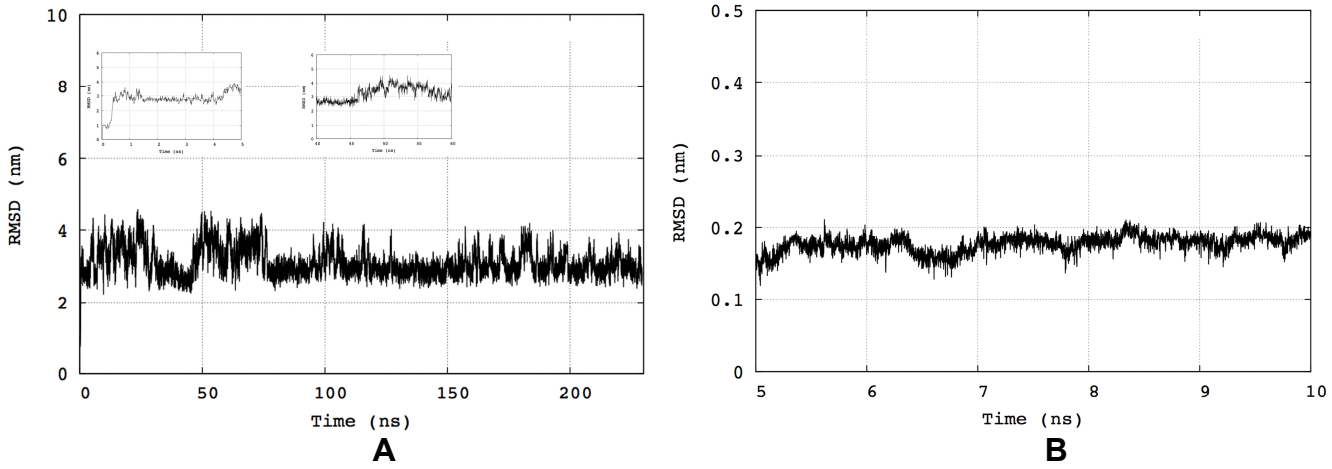

Figure S2. RMSD for the (panel A) 230ns MD simulation of CSA and (panel B) 10ns MD simulations of the CAPN2 target. The two inserts at the top of panel A show the beginning and the middle of the simulation.

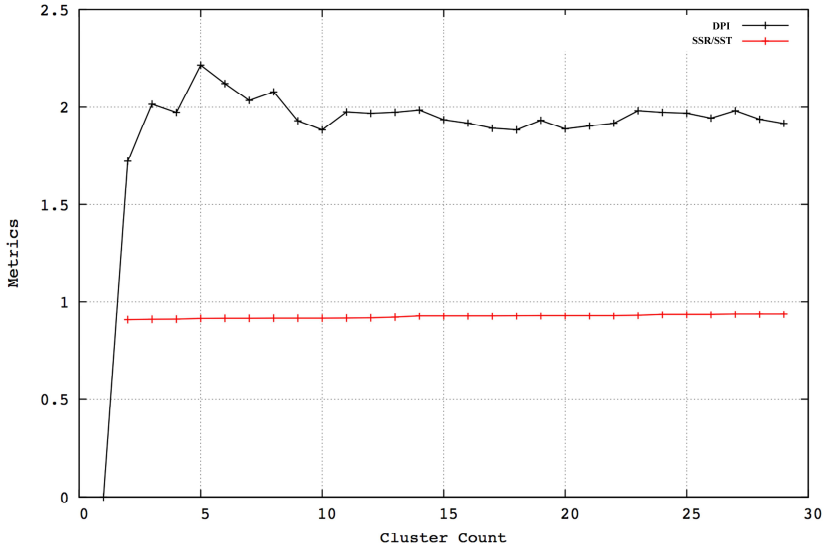

Figure S3. Clustering analysis for the 230ns MD simulation of CSA.

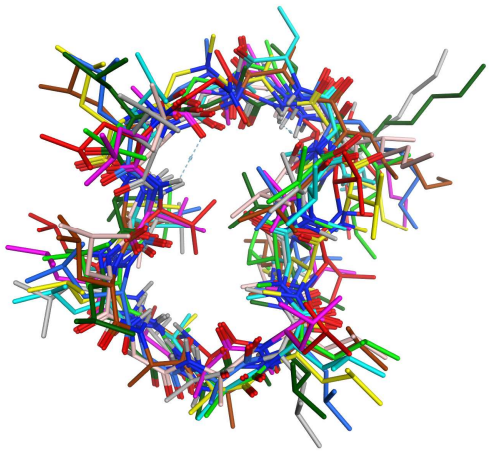

Figure S4. The ten dominant conformations of CSA found based on clustering of the 230ns MD simulation.

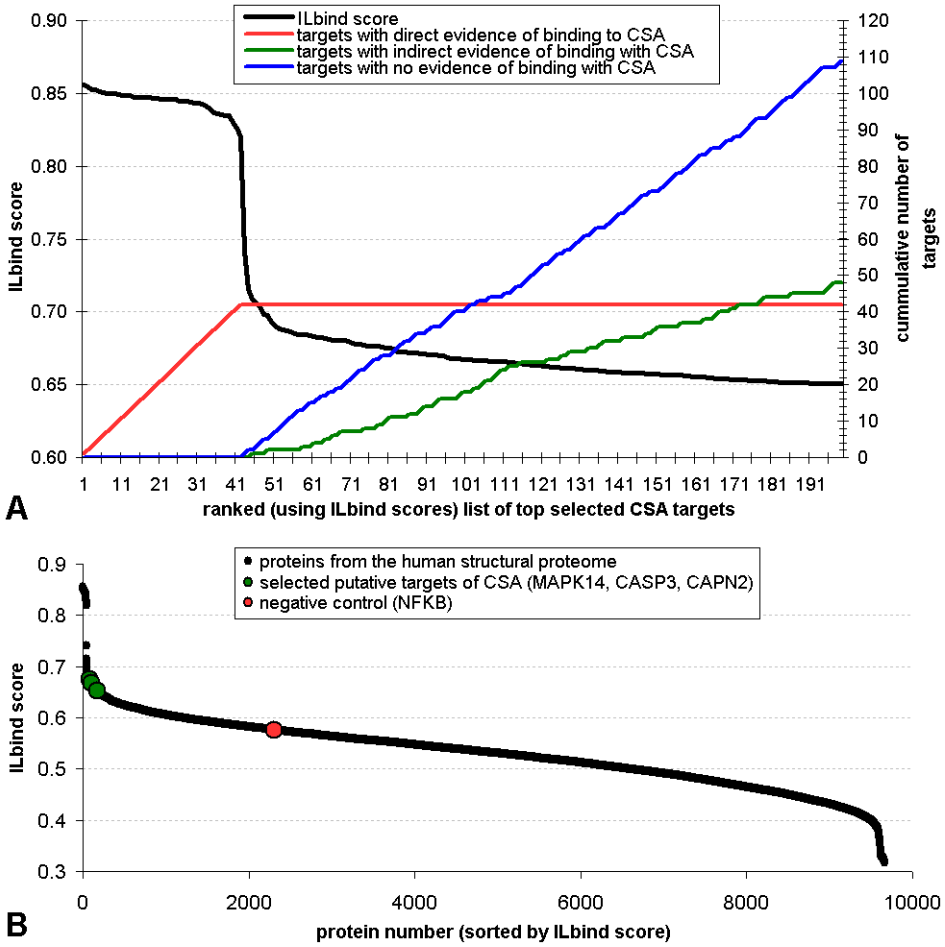

Figure S5. Overview of the ILbind scores and fraction of targets with evidence of binding to CSA. Panel A shows cumulative number of putative CSA targets identified by ILbind that are annotated as supported by direct evidence of binding to CSA (based on PDB, BindingDB and DrugBank), indirect evidence (they are associated with CSA in a publication found in PUBMED), or otherwise as having no evidence of binding to CSA for the top 199 targets identified with ILbind. Panel B gives the ILbind scores for all proteins from the structural human proteome. The *x*-axes in both panels sort the targets according the ILbind scores.

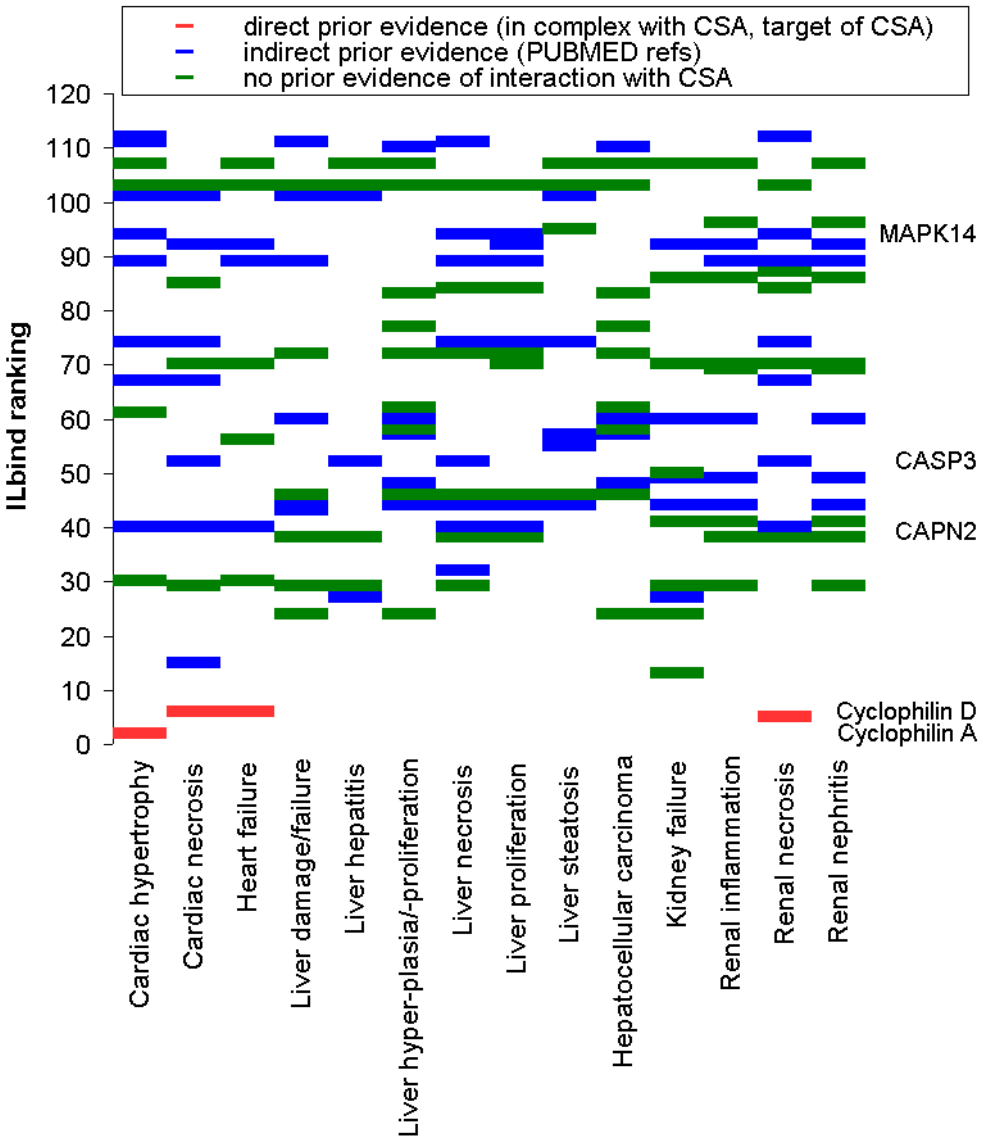

Figure S6. Association of putative CSA targets and the corresponding toxic responses that they are involved in based on results generated by Ingenuity release 2012-11-01. The *x*-axis lists toxic responses grouped by the corresponding organs including heart, liver, and kidneys. The *y*-axis shows the rank of the corresponding targets that is denoted by a color-coded horizontal line, where red denotes targets supported by direct evidence, blue by indirect evidence, and green denotes targets that are annotated as having no prior evidence for interaction with CSA.

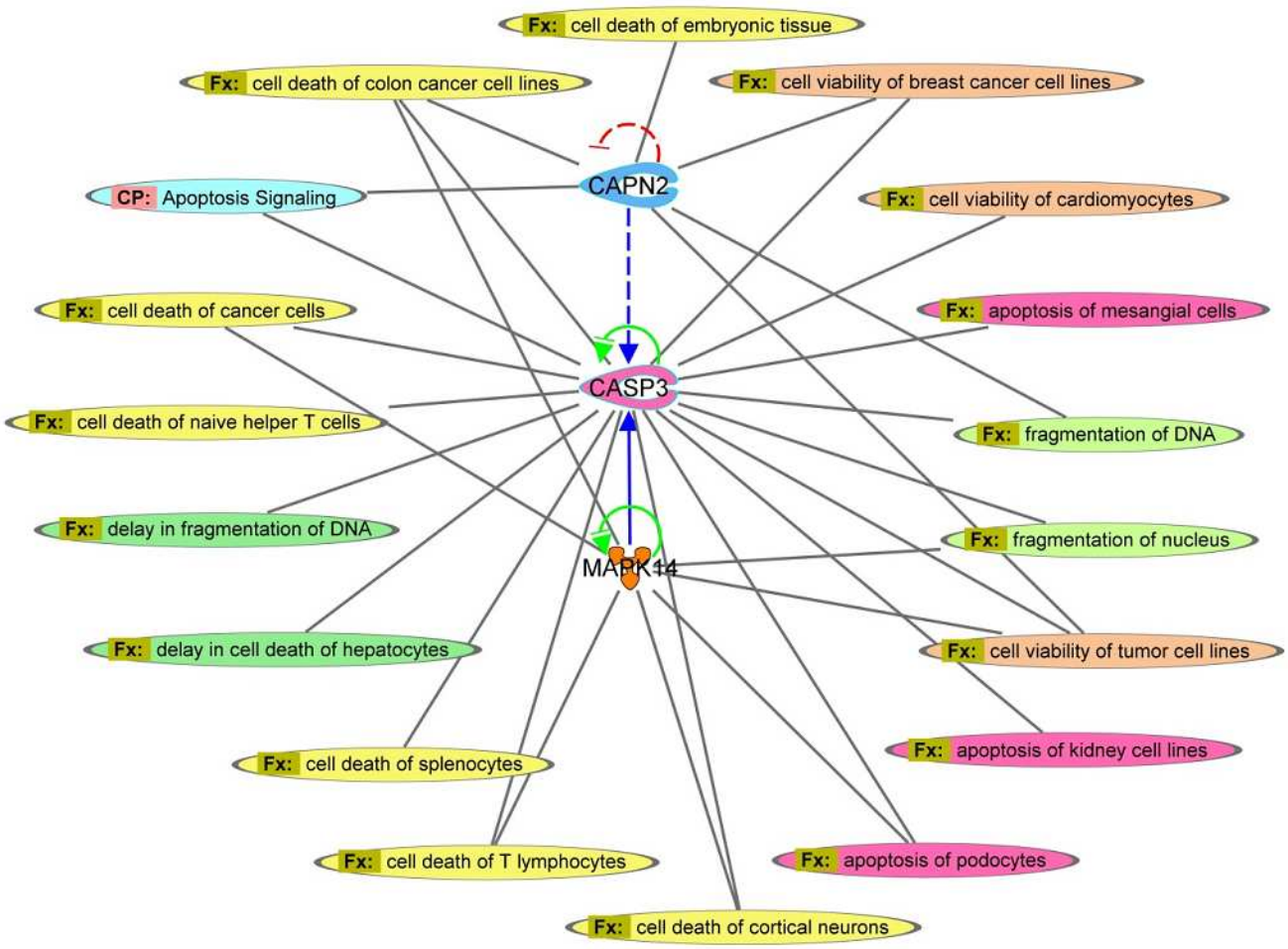

Figure S7. Analysis of calpain 2 (CAPN2), p38 MapK (MAPK14) and caspase 3 (CASP3) interactions generated by Ingenuity release 2012-11-01 to identify connections with apoptotic pathways. Blue solid arrow: direct relationship; blue dashed arrow: indirect relationship; green arrow: self-activating; red dashed line: self-inhibitory. The associated artifacts include canonical pathways (CP) and functions (Fx) that are color-coded: yellow: cell death; green: delay; orange: cell viability; light blue: apoptosis signaling; pink: apoptosis; and light green: fragmentation.

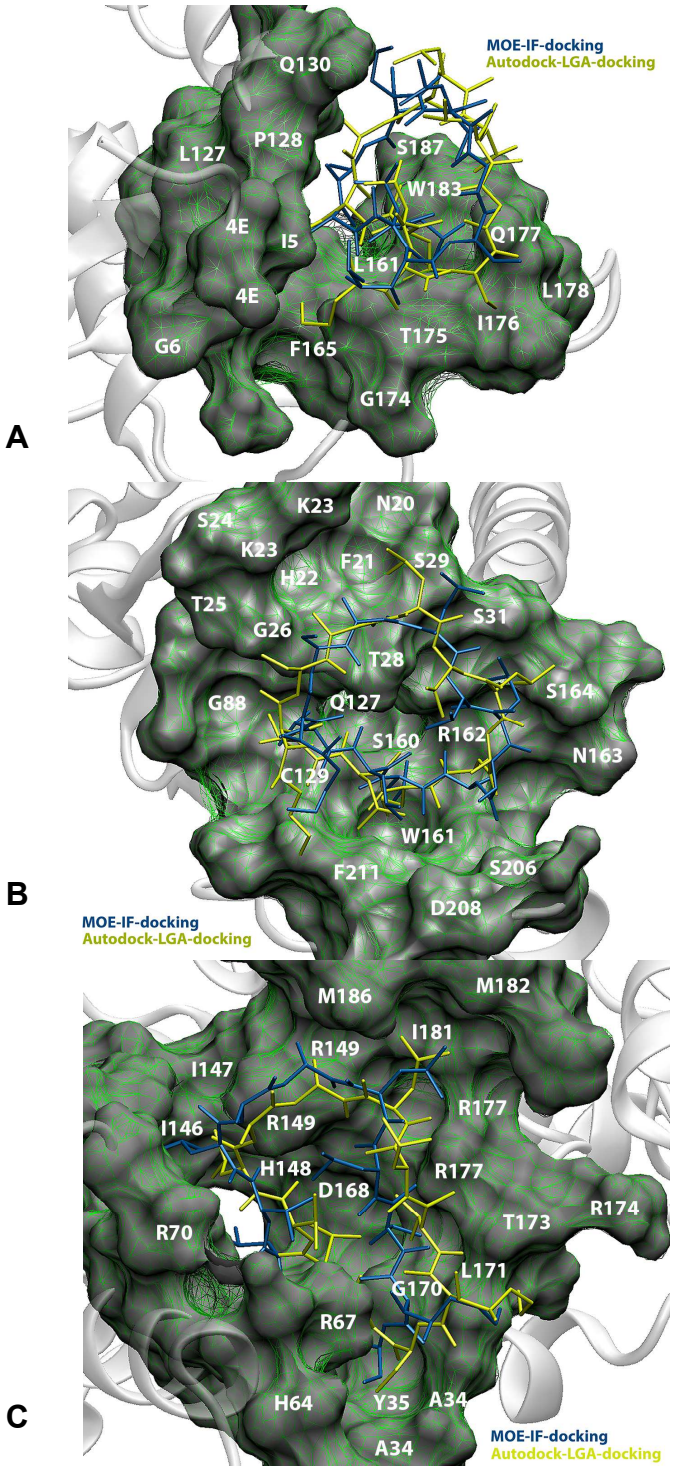

Figure S8. The mode of binding of CSA using two docking methods for CAPN2 (PDBid 3bow_A; panel A), CASP3 (4ehl_A, panel B), and MAPK14 (3zs5_A, panel C). The poses generated with AUTODOCK and MOE are shown in yellow and blue, respectively. The binding pocket is shown as a surface representation in grey enhanced with a green wireframe.

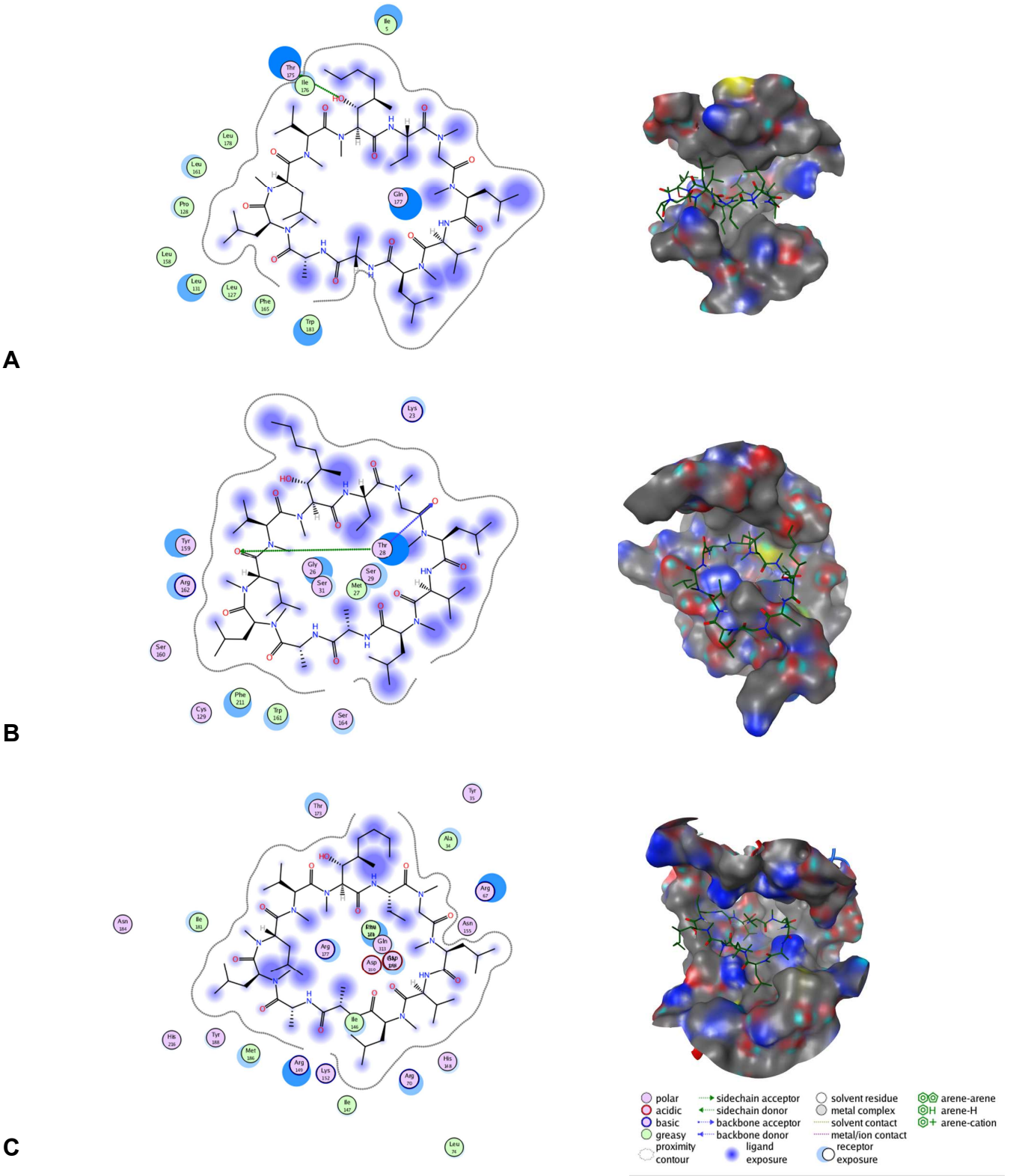

Figure S9. Binding modes (poses) of CSA for the four putative targets: CAPN2 (PDBid 3bow_A; panel A), CASP3 (4ehl_A, panel B), and MAPK14 (3zs5_A, panel C). The images on the right show the 3-D conformation of the CSA in the binding site on a given target with interacting residues shown as surface colored by their atomic structure (C in gray, O in red, N in blue and H in white). CSA is shown in licorice following the same color codes, except C is shown in green. The images on the left illustrate atomic interactions of CSA with the residues of the target. The interactions are color coded as shown in the figure legend at the bottom.

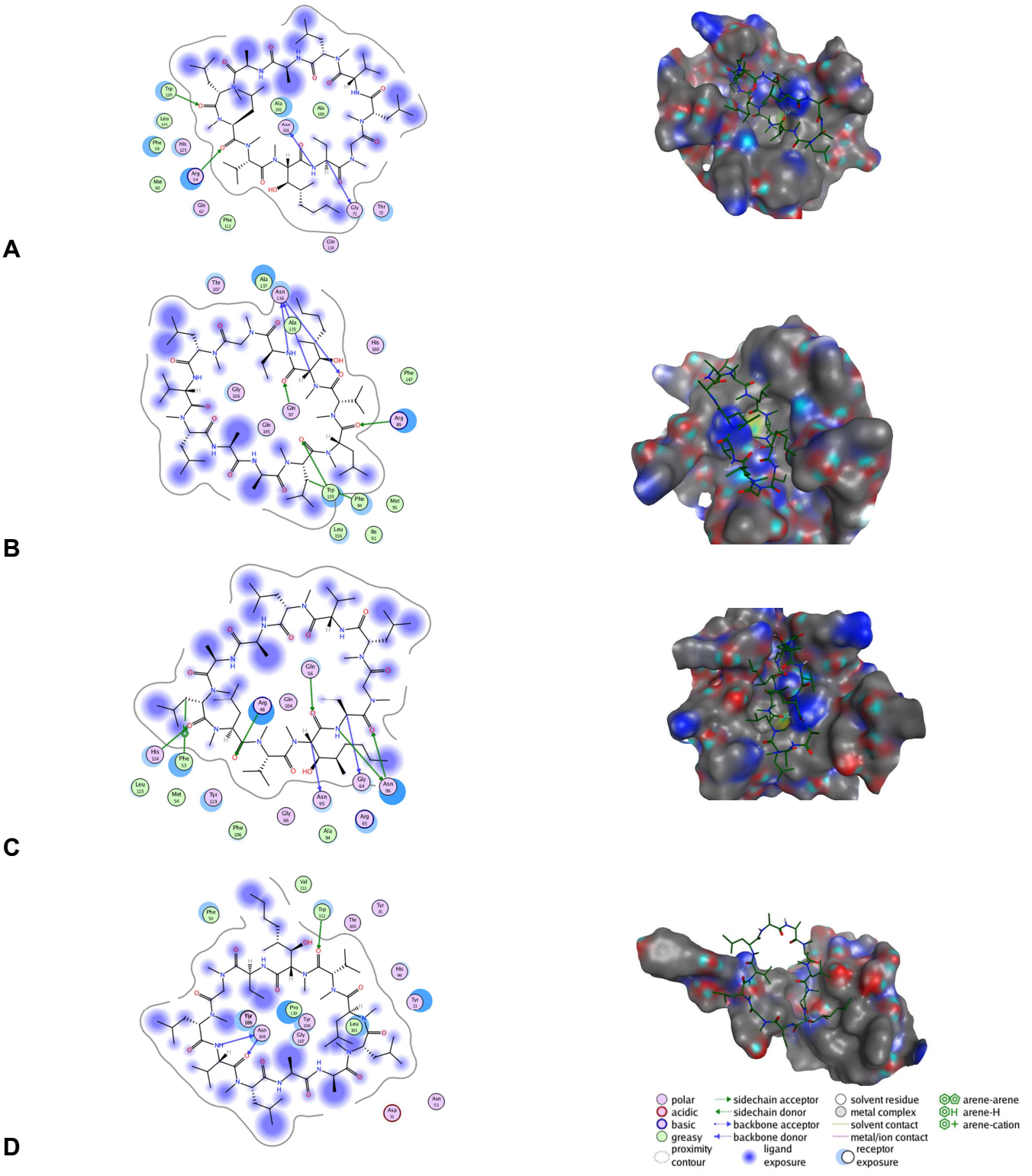

Figure S10. Binding modes (poses) of CSA for the four representative positive controls: Cyclophilin A (PDBid: 3pmp_B; panel A), Cyclophilin C (2rmc_A; panel B), cyclophilin-like protein (2oju_A; panel C), and FAB fragment IGG1-kappa (1ikf_H; panel D). The four images on the right show the 3-dimensional conformation of the CSA in the binding site on a given target. The interacting residues are shown as surface colored by their atomic structure (C in gray, O in red, N in blue and H in white). CSA is shown in licorice representation following the same color codes, except C shown in green. The images on the left illustrate atomic interactions of CSA with the residues of the target. The interactions are color coded as shown in the figure legend at the bottom.

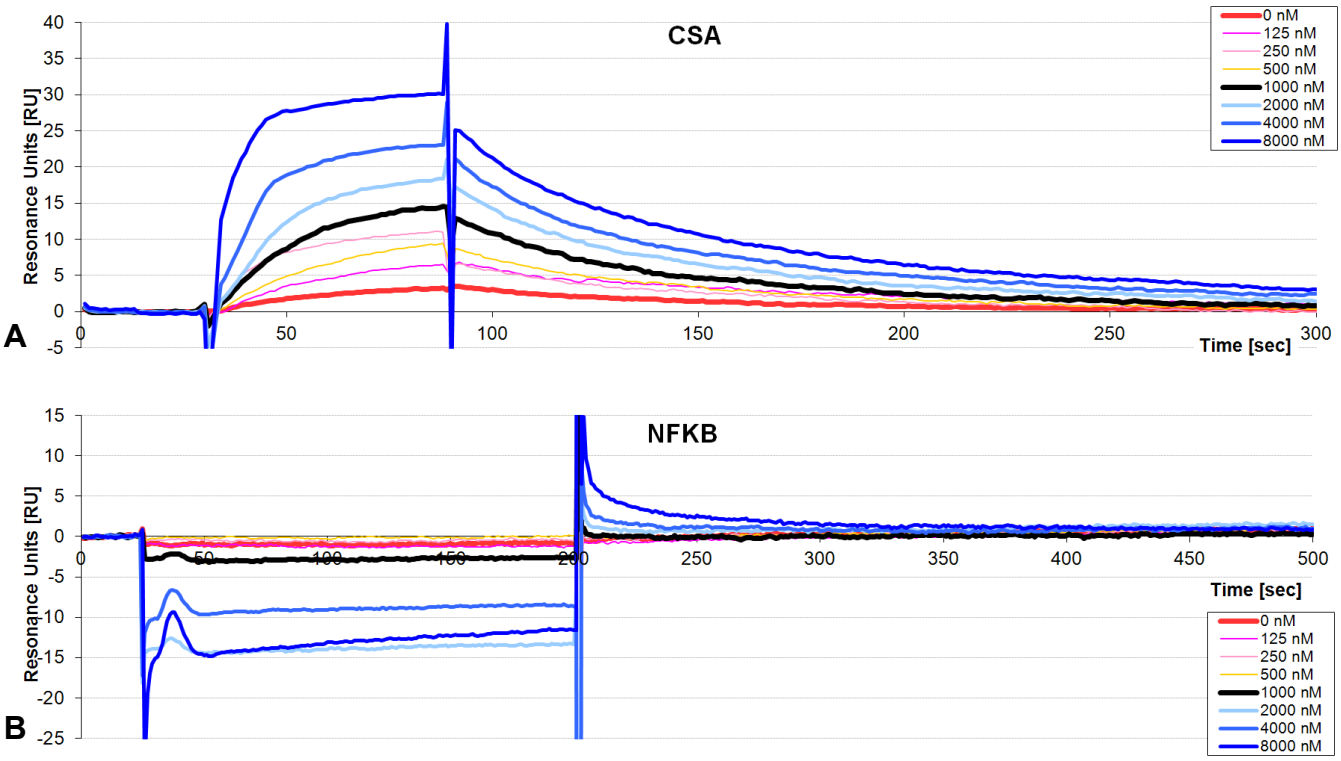

Figure S11. Real-time sensorgrams to measure interactions of CSA at 8000, 4000, 2000, 1000, 500, 250, 125 and 0 nM concentration with positive control cyclophilin A (CSA; panel A) and negative control NF-kappa B p65 (NFKB; panel B). The sensorgrams were averaged over three repetitions.

Supplementary Table S1. Detailed characterization of the selected 199 putative targets of CSA. The targets proteins are sorted by the ILbind score in the descending order. The information includes protein name, PDB and UniProt identifiers, ILbind score, annotation of type of evidence of interaction with CSA (if any), and annotation of the associated toxicities collected using Ingenuity release 2012-11-01 (http://www.ingenuity.com/); the "used to analyze toxicity" indicates which target proteins were successfully mapped to Ingenuity to perform the analysis. The toxicities are abbreviated as follows: cardiac hypertrophy (CH), cardiac necrosis (CN), heart failure (HF), liver damage/failure (LD), liver hepatitis (LH), liver hyper-plasia/-proliferation (LHP), liver necrosis (LN), liver proliferation (LP), liver steatosis (LS), hepatocellular carcinoma (HC), kidney failure (KF), renal inflammation (RI), renal necrosis (RN), and renal nephritis (RH).

PDBid	UniProtID	Name [abbreviated name]	In complex with CSA	Used as template	ILbind score	Evidence of interaction with CSA: direct (in complex with CSA or known target); indirect (via PUBMED references IDs); and none	Used to analyze toxicity	Found to be associated with toxicity												
								CH	CN	HF	LD	LH	LHP	LN	LP	LS	HC	KF	RI	RN	RH
2esl_A	P45877	Cyclophilin C [PPIC]	Y		0.856	direct	Y													
1c5f_C	Q27450	Cyclophilin-like [PPIL2]	Y	Y	0.855	direct														
2x2a_A	P62937	Cyclophilin A [PPIA]	Y		0.852	direct	Y	x												
2x25_B	P62937	Cyclophilin A [PPIA]	Y		0.852	direct	Y	x												
1mik_A	P62937	Cyclophilin A [PPIA]	Y	Y	0.851	direct	Y	x												
2alf_A	P62937	Cyclophilin A [PPIA]	Y		0.850	direct	Y	x												
3k0m_A	P62937	Cyclophilin A [PPIA]	Y		0.850	direct	Y	x												
2xgy_B	P62937	Cyclophilin A [PPIA]	Y		0.850	direct	Y	x												
3k0o_A	P62937	Cyclophilin A [PPIA]	Y		0.850	direct	Y	x												
1qng_A	Q25756	Cyclophilin A [PPIA]	Y	Y	0.849	direct	Y	x												
2oju_A	Q9H2H8	Cyclophilin-like [PPIL3]	Y	Y	0.849	direct	Y													
3uch_A	Q9UNP9	Cyclophilin E [PPIE]	Y		0.849	direct	Y													
2ok3_A	Q9H2H8	Cyclophilin-like [PPIL3]	Y		0.848	direct	Y													
2x83_B	B0ZE32	TRIMcyp (has PPIA domain) [TRIMC]			0.847	direct														
1ihg_A	P26882	Cyclophilin D [PPID]			0.847	direct	Y													x
2z6w_A	P30405	Cyclophilin F [PPIF]	Y	Y	0.847	direct	Y		x	x										
1zmf_A	Q9UNP9	Cyclophilin E [PPIE]	Y		0.847	direct	Y													
2poy_C	A3FQA7	Cyclophilin A [PPIA]	Y	Y	0.847	direct	Y	x												
3k0r_A	P62937	Cyclophilin A [PPIA]	Y		0.847	direct	Y	x												
2wlw_A	P62940	TRIMcyp (has PPIA domain) [TRIMC]	Y		0.847	direct	Y													
3pmp_B	E3P6K5	Cyclophilin A [PPIA]	Y	Y	0.846	direct	Y	x												
3rdd_A	P62937	Cyclophilin A [PPIA]	Y		0.846	direct	Y	x												
1awq_A	P62937	Cyclophilin A [PPIA]	Y		0.846	direct	Y	x												
2bit_X	P30405	Cyclophilin D [PPID]	Y		0.846	direct	Y		x	x										
1m9e_A	P62937	Cyclophilin A [PPIA]	Y		0.846	direct	Y	x												
2r99_A	Q9UNP9	Cyclophilin E [PPIE]	Y		0.845	direct	Y													
3qyu_A	P30405	Cyclophilin F [PPIF]	Y		0.845	direct	Y		x	x										
2a2n_A	Q96BP3	Peptidylprolyl isomerase [PPWD1]	Y		0.844	direct	Y													
4dgd_A	P62940	TRIMcyp (has PPIA domain) [TRIMC]			0.844	direct	Y													

PDBid	UniProtID	Name [abbreviated name]	In complex with CSA	Used as template	ILbind score	Evidence of interaction with CSA: direct (in complex with CSA or known target); indirect (via PUBMED references IDs); and none	Used to analyze toxicity	Found to be associated with toxicity													
								CH	CN	HF	LD	LH	LHP	LN	LP	LS	HC	KF	RI	RN	RH
1mzw_A	O43447	Cyclophilin H [PPIH]			0.844	direct	Y														
2rmc_A	P30412	Cyclophilin C [PPIC]	Y	Y	0.843	direct	Y														
3rcg_A	P30405	Cyclophilin F [PPIF]	Y		0.843	direct	Y		x	x											
3eov_B	Q9U9R3	Cyclophilin A [PPIA]	Y	Y	0.841	direct	Y	x													
3ich_A	P23284	Cyclophilin B [PPIB]	Y		0.839	direct	Y														
1ikf_H		FAB fragment IGG1-kappa (heavy chain) [FABIGG1K]	Y	Y	0.837	direct															
3bo7_C	D0VWS5	Cyclophilin-like [PPIL4]	Y	Y	0.836	direct															
2wfi_A	Q13427	Cyclophilin G [PPIG]	Y		0.835	direct	Y														
1cyn_A	P23284	Cyclophilin B [PPIB]	Y	Y	0.835	direct	Y														
2x7k_A	Q9Y3C6	Cyclophilin-like [PPIL1]	Y	Y	0.834	direct	Y														
2gw2_A	Q13427	Cyclophilin G [PPIG]	Y		0.830	direct	Y														
2wfj_A	Q13427	Cyclophilin G [PPIG]	Y	Y	0.826	direct	Y														
1xq7_B	Q4DPB9	Cyclophilin A [PPIA]	Y	Y	0.820	direct	Y	x													
1dfb_H	P01857	FAB fragment IGG1-kappa (heavy chain) [IGHG1]			0.742	none	Y											x			
3h42_H	Q8NBP7	Proprotein convertase subtilisin/kexin type 9 [PCSK9]			0.715	none	Y														
3gd4_A	Q9Z0X1	Apoptosis-inducing factor [AIFM1]			0.709	indirect (12787063)	Y		x												
1qr6_A	P23368	Malic enzyme 2 [ME2]			0.706	none	Y														
3pff_A	P53396	ATP citrate lyase [ACLY]			0.704	none	Y														
3eo9_H		FAB fragment Efalizumab (heavy chain) [FABEFZ]			0.698	none															
2v1x_A	P46063	DNA helicase Q1 [RECQL]			0.697	indirect (21559518)	Y														
2qzl_A	P56817	Beta-secretase 1 [BACE1]			0.693	none	Y														
4ei1_A	Q9UKV8	Protein argonaute-2 [EIF2C2]			0.690	none	Y														
3c2a_L	P0CG05	Immunoglobulin lambda constant 2 [IGLC2]			0.689	none	Y														
2ch5_A	Q9UJ70	N-acetylglucosamine kinase [NAGK]			0.688	none	Y														
2www_A	Q8IVH4	Methylmalonic aciduria type A [MMAA]			0.687	none	Y														
1zxm_A	P11388	DNA topoisomerase II alpha [TOP2A]			0.687	none	Y				x		x				x	x			
3hlk_A	P49753	Acyl-CoA thioesterase 2 [ACOT2]			0.685	none	Y														
2bra_A	Q8VDP3	Microtubule associated monoxygenase [MICAL1]			0.685	none	Y														
1kgu_A	P04746	Alpha amylase [AMY2A]			0.685	indirect (7504818)	Y					x						x			
3thx_B	P20585	DNA mismatch repair protein [MSH3]			0.684	none	Y														
2vxs_H	Q16552	Interleukin 17A [IL17A]			0.684	none	Y		x		x	x		x				x	x		x
3a5m_C	P07830	Filamentous actin [FACT]			0.683	indirect (18724379)															
3duy_A	P56817	Beta-secretase 1 [BACE1]			0.683	none	Y														
3tpp_A	P56817	Beta-secretase 1 [BACE1]			0.683	none	Y														

PDBid	UniProtID	Name [abbreviated name]	In complex with CSA	Used as template	ILbind score	Evidence of interaction with CSA: direct (in complex with CSA or known target); indirect (via PUBMED references IDs); and none	Used to analyze toxicity	Found to be associated with toxicity												
								CH	CN	HF	LD	LH	LHP	LN	LP	LS	HC	KF	RI	RN	RH
1ad0_B		FAB fragment A5B7 (heavy chain) [FABA5B7]			0.682	indirect (2004846)															
4anw_A	P48736	Phosphoinositide 3-kinase [PIK3CG]			0.681	none	Y	x		x											
2vgg_A	P30613	Pyruvate kinase [PKLR]			0.681	indirect (22580449)	Y														
3lrs_L		FAB fragment PG16 (light chain) [FABPG16]			0.681	none															
3tlm_A	Q0VCY0	Calcium ATPase 1 [ATP2A1]			0.680	indirect (12022919)	Y							x							
2d3v_A	A6NI73	Leukocyte immunoglobulin-like receptor [LILRA5]			0.680	none	Y														
3eh1_A	O95487	Transport protein Sec24B [SEC24B]			0.680	none	Y														
3ek8_A	P42212	Myosin light chain kinase [SEC24B]			0.679	none															
3ekh_A	P42212	Myosin light chain kinase [SEC24B]			0.678	none															
3caa_A	P01011	Antichymotrypsin [SERPINA3]			0.678	none	Y														
2obd_A	P11597	Cholesteryl ester transfer protein [CETP]			0.677	indirect (18448283)	Y														
3mlu_L	Q9J0Z7	FAB fragment 2557 (light chain) [FAB2557]			0.677	none															
1dcl_A	P01709	Immunoglobulin light chain dimer [MCG]			0.677	none															
3skj_H	P29317	FAB fragment IGG1-kappa (heavy chain) [EPHA2]			0.676	none	Y														
2zxe_A	Q4H132	K-ATPase alpha [KATPA]			0.676	indirect (7711433)															
3thm_L	P25445	FAB fragment EP6b (light chain) [FAS]			0.676	none	Y				x	x		x	x				x	x	x
1df0_A	Q07009	Calpain 2 [CAPN2]			0.675	indirect (21980535)	Y														
3aln_A	P45985	Mitogen-activated kinase 4 [MAP2K4]			0.675	indirect (22147139)	Y	x	x	x				x	x					x	
1l7i_H		Chimera of FAB2C4 [FAB2C4]			0.675	none															
3u0p_A	P15813	Antigen-presenting glycoprotein CD1d [CD1D]			0.673	none	Y											x	x		x
1t5c_A	Q02224	Centromeric protein E [CENPE]			0.672	none	Y														
1o1n_A	P69905	Hemoglobin alpha [HEMA]			0.672	none															
3bow_A	Q07009	Calpain 2 [CAPN2]			0.672	indirect (21980535)	Y														
3mlx_L	P05877	FAB fragment 3074 (light chain) [FAB3074]			0.672	none															
3mlr_L	P12490	FAB fragment 2557 (light chain) [FAB2557]			0.672	none															
3tmi_A	O95786	ATP-dependent RNA helicase [DDX58]			0.672	indirect (21559518)	Y				x										
2hr0_A	P01024	Complement C3 beta [C3]			0.671	indirect (19070591;12234299)	Y				x		x	x	x	x		x	x		x
3p7o_A	P35559	Insulin-degrading enzyme [IDE]			0.671	none	Y														
3uji_L	P05877	FAB fragment 2558 (light chain) [FAB2558]			0.670	none															
1d4x_A	P10983	Actin [ACT]			0.670	indirect (18724379)															
2fgh_A	Q28372	Gelsolin [GELS]			0.670	indirect (17615162)															
3c08_H	P01857	FAB fragment Matuzumab (heavy chain) [IGHG1]			0.670	none	Y											x			
3mlv_L	Q79790	FAB fragment 2557 (light chain) [FAB2557]			0.669	none															
1osh_A	Q96RI1	Bile acid receptor [NR1H4]			0.668	none	Y				x		x	x	x	x	x				
1mkj_A	P33176	Kinesin motor domain [KIF5B]			0.668	none	Y														

PDBid	UniProtID	Name [abbreviated name]	In complex with CSA	Used as template	ILbind score	Evidence of interaction with CSA: direct (in complex with CSA or known target); indirect (via PUBMED references IDs); and none	Used to analyze toxicity	Found to be associated with toxicity												
								CH	CN	HF	LD	LH	LHP	LN	LP	LS	HC	KF	RI	RN	RH
1hx1_A	P19120	Heat shock 70 kDa protein 8 [HSPA8]			0.668	indirect (21558416;19664129)	Y						x				x				
2ok5_A	P00751	Complement factor B [CFB]			0.668	indirect (19070591;12234299)	Y											x	x		x
1hzh_H	P01857	Immunoglobulin heavy chain [IGHG1]			0.667	none	Y											x			
2hi9_A	P05154	Serine protease inhibitor [SERPINA5]			0.667	none	Y														
4ehn_A	P42574	Caspase 3 [CASP3]			0.667	indirect (22790389;12787063)	Y		x			x		x						x	
3tbd_A	Q96CW9	Netrin G2 [NTNG2]			0.667	none	Y														
3d2f_B	P08107	Heat shock 70 kDa protein 1 [HSPA1]			0.666	indirect (21558416;19664129)															
2pm8_A	P06276	Cholinesterase [BCHE]			0.666	indirect (17467222;12633900)	Y														
3tje_L	P25445	FAB fragment E09 (light chain) [FAS]			0.666	none	Y				x	x		x	x				x	x	x
3hrz_D	P00751	Complement factor B [CFB]			0.666	indirect (19070591;12234299)	Y											x			x
3dtb_A	P07379	Phosphoenolpyruvate carboxykinase [PCK1]			0.666	indirect (1618871;19252740)	Y									x					
1qx3_A	P42574	Caspase 3 [CASP3]			0.666	indirect (22790389;12787063)	Y		x			x		x						x	
4d8o_A	Q01484	Ankyrin 2 [ANK2]			0.666	none	Y			x											
3qfc_A	P16435	Cytochrome P450 reductase [POR]			0.665	indirect (2277139)	Y						x			x	x				
2wgh_A	P23921	Ribonucleotide reductase M1 [RRM1]			0.665	none	Y						x				x				
2b5l_A	Q16531	Damage-specific DNA binding protein 1 [DDB1]			0.665	none	Y														
2vdb_A	P02768	Albumin [ALB]			0.664	indirect (22016592)	Y				x		x				x	x	x		x
3mlw_L	P05877	FAB fragment 1006-15D (light chain) [FAB1006]			0.664	none															
1q47_A	O08665	Semaphorin 3A [SEMA3A]			0.664	none	Y	x													
3g0f_A	P10721	Receptor tyrosine kinase [KIT]			0.664	none	Y						x				x				
2qs9_A	O75884	Retinoblastoma-binding protein 9 [RBBP9]			0.663	none	Y														
3eh2_A	P53992	Transport protein SEC24C [SEC24C]			0.663	none	Y														
3hgz_A	P14735	Insulin-degrading enzyme [IDE]			0.663	none	Y														
3qe2_A	P16435	Cytochrome P450 reductase [POR]			0.663	indirect (2277139)	Y						x			x	x				
1i5s_A	P33173	Kinesin-like protein [KIF1A]			0.662	none	Y														
8fab_A		FAB fragment IGG1-lambda (light chain) [FABIGG1L]			0.662	none															
3u9h_A	Q9H2K2	Tankyrase 2 [TNKS2]			0.662	none	Y														
1t44_A	P06396	Gelsolin domain 1 [GSN]			0.662	indirect (18724379)	Y	x	x											x	
3egd_A	Q15436	Transport protein SEC23A [SEC23A]			0.661	none	Y														
3n5k_A	P04191	Calcium ATPase 1 [ATP2A1]			0.661	indirect (12022919)	Y							x							

PDBid	UniProtID	Name [abbreviated name]	In complex with CSA	Used as template	ILbind score	Evidence of interaction with CSA: direct (in complex with CSA or known target); indirect (via PUBMED references IDs); and none	Used to analyze toxicity	Found to be associated with toxicity												
								CH	CN	HF	LD	LH	LHP	LN	LP	LS	HC	KF	RI	RN	RH
1sq0_B	P07359	Glycoprotein Ib alpha [GP1BA]			0.661	none	Y												x		x
1rz7_L		FAB fragment 48d (light chain) [FAB48d]			0.661	none															
2jgz_A	P24941	Cyclin-dependent kinase 2 [CDK2]			0.661	none	Y		x	x					x			x	x	x	x
2omn_A		Immunoglobulin light chain [IGL]			0.660	none															
1d0n_A	Q28372	Gelsolin [GELS]			0.660	indirect (17615162)															
3bho_A	O43809	Cleavage factor I(m)25 [NUDT21]			0.660	none	Y														
3q6w_A	P08581	Hepatocyte growth factor receptor [MET]			0.660	none	Y				x		x	x	x		x				
3ov6_A	P29016	T-cell surface glycoprotein CD1b [CD1B]			0.660	indirect (22696872)	Y														
3o96_A	P31749	RAC-alpha serine/threonine-protein kinase [AKT1]			0.659	indirect (14576824;14527673)	Y	x	x					x	x	x				x	
3ohm_B	Q01970	Phospholipase C beta 3 [PLCB3]			0.659	none	Y														
2v26_A	Q29122	Myosin VI [MYO6]			0.659	none															
3ghe_L		FAB fragment 537-10D (light chain) [FAB537]			0.659	none															
1gte_A	Q28943	Dihydroprymidine dehydrogenase [DHPDH]			0.659	none															
3m6g_A	P68135	Actin alpha [ACTA]			0.658	indirect (18724379)															
1yjl_A	P14925	Peptidyl-glycine alpha-amidating monooxygenase [PAM]			0.658	none	Y														
3tuv_A	P35559	Insulin-degrading enzyme [IDE]			0.658	none	Y														
3u2s_L	Q6TCP8	FAB fragment PG9 (light chain) [FABPG9]			0.658	none															
3t6b_A	Q9NY33	Dipeptidyl peptidase 3 [DPP3]			0.658	none	Y						x				x				
3map_A	O75874	Isocitrate dehydrogenase [IDH1]			0.658	none	Y														
3mdm_A	Q9Y6A2	Cytochrome P450 46A1 [CYP46A1]			0.658	indirect (2277139)	Y														
1t77_A	P50851	LPS-responsive vesicle [LRBA]			0.657	none	Y														
1tf0_A	P02768	Albumin [ALB]			0.657	indirect (22016592)	Y				x		x				x	x	x		x
1f13_A	P00488	Coagulation factor XIII [F13A1]			0.657	indirect (21938677)	Y														
1abb_A	P00489	Blycogen phosphorylase b [GPb]			0.657	none															
3l1b_A	Q96RI1	Bile acid receptor [NR1H4]			0.657	none	Y				x		x	x	x	x	x				
1olm_A	O76054	SEC14-like protein 2 [SEC14L2]			0.657	none	Y														
4dt6_A	P06730	Eukaryotic translation initiation factor 4E [EIF4E]			0.657	none	Y						x				x				
3ije_A	P06756	Integrin alpha-V [ITGAV]			0.657	none	Y							x	x					x	
4ehl_A	P42574	Caspase 3 [CASP3]			0.656	indirect (22790389;12787063)	Y		x			x		x						x	
1nxk_A	P49137	MAP kinase-activated protein kinase 2 [MAPKAPK2]			0.656	none	Y		x												
1zvd_A	Q9HAU4	SMAD ubiquitination regulatory factor 2 [SMURF2]			0.656	none	Y												x	x	x
3cx6_A	P27601	Guanine nucleotide-binding protein alpha 13 [GNA13]			0.656	none	Y													x	
3efo_A	Q15436	Transport protein SEC23A [SEC23A]			0.655	none	Y														
2a1u_A	P13804	Electron transfer flavoprotein alpha [ETFA]			0.655	none	Y														

PDBid	UniProtID	Name [abbreviated name]	In complex with CSA	Used as template	ILbind score	Evidence of interaction with CSA: direct (in complex with CSA or known target); indirect (via PUBMED references IDs); and none	Used to analyze toxicity	Found to be associated with toxicity												
								CH	CN	HF	LD	LH	LHP	LN	LP	LS	HC	KF	RI	RN	RH
2o61_B	P19838	Nuclear factor NF-kappa-B p105 subunit [NFKB1]			0.655	indirect (2595372)	Y	x		x	x			x	x				x	x	x
3kdm_H		Immunoglobulin heavy chain [IGH]			0.655	none															
2iwi_A	Q9P1W9	Sserine/threonine kinase PIM-2 [PIM2]			0.655	none	Y														
2j33_A	P42574	Caspase 3 [CASP3]			0.654	indirect (22790389;12787063)	Y		x			x		x						x	
3pd1_A	P42574	Caspase 3 [CASP3]			0.654	indirect (22790389;12787063)	Y		x			x		x						x	
3so3_C	Q9Y5Y6	FAB fragment A11 (heavy chain) [ST14]			0.654	none	Y														
3i25_A	P56817	Beta-secretase 1 [BACE1]			0.654	none	Y														
1wyg_A	P22985	Xanthine dehydrogenase/oxidase [XDH]			0.654	indirect (17761348;17603163)	Y		x	x					x			x	x		x
2e26_A	Q60841	Reelin [RELN]			0.654	none	Y														
3zs5_A	Q16539	p38 mitogen-activated protein kinase 14 [MAPK14]			0.653	indirect (22917034;22678567; 21912224)	Y	x						x	x					x	
3fe3_A	P27448	MAP/microtubule affinity-regulating kinase 3 [MARK3]			0.653	none	Y									x					
1pg7_H	P01863	FAB fragment D3H44 (heavy chain) [Ighg2a]			0.653	none	Y												x		x
3r1g_B	P56817	Beta-secretase 1 [BACE1]			0.653	none	Y														
1a6z_A	Q30201	Hemochromatosis [HFE]			0.653	none	Y														
1o6g_A	P23687	Prolyl oligopeptidase [PLOP]			0.653	none															
2e3t_A	P22985	Xanthine dehydrogenase/oxidase [XDH]			0.653	indirect (17761348;17603163)	Y		x	x					x			x	x		x
3lc3_A	P00740	Coagulation factor IX [F9]			0.653	indirect (1639529)	Y														
2g75_B		FAB fragment m396 (light chain) [FABm396]			0.652	none															
1fdw_A	P14061	17-beta hydroxysteroid dehydrogenase 1 [HSD17B1]			0.652	none	Y														
3ean_A	O89049	Thioredoxin reductase 1 [TXNRD1]			0.652	none	Y														
2g47_A	P14735	Insulin-degrading enzyme [IDE]			0.652	none	Y														
3gjf_L		FAB fragment (light chain) [FABTCR]			0.652	none															
3efo_B	O94855	Transport protein SEC24D [SEC24D]			0.652	none	Y														
2shp_A	Q06124	Tyrosine phosphatase SHP-2 [PTPN11]			0.652	indirect (16297055)	Y	x	x		x	x				x					
3elj_A	P45983	Mitogen-activated protein kinase 8 [MAPK8]			0.651	none	Y	x	x	x	x	x	x	x	x	x	x			x	
3lra_A	Q12959	Disks large homolog 1 [DLG1]			0.651	none	Y														
2xtj_A	Q8NBP7	Proprotein convertase subtilisin/kexin type 9 [PCSK9]			0.651	none	Y														
2f2u_A	Q28021	Rho-associated protein kinase 2 [ROCK2]			0.651	none	Y														
3thx_A	P43246	DNA mismatch repair protein Msh2 [MSH2]			0.651	none	Y														
3lfv_A	O76074	cGMP-specific phosphodiesterase [PDE5A]			0.651	none	Y	x		x		x	x			x	x	x	x		x
1xoi_A	P06737	Glycogen phosphorylase [PYGL]			0.651	none	Y														

PDBid	UniProtID	Name [abbreviated name]	In complex with CSA	Used as template	ILbind score	Evidence of interaction with CSA: direct (in complex with CSA or known target); indirect (via PUBMED references IDs); and none	Used to analyze toxicity	Found to be associated with toxicity												
								CH	CN	HF	LD	LH	LHP	LN	LP	LS	HC	KF	RI	RN	RH
2oni_A	Q96PU5	E3 ubiquitin-protein ligase [NEDD4L]			0.651	none	Y													
2hf3_A	P10987	Actin 5C [ACTG1]			0.651	indirect (18724379)	Y						x				x			
1gmy_A	P07858	Cathepsin B [CTSB]			0.651	indirect (15324353)	Y	x			x			x						
2al6_A	Q00944	Focal adhesion kinase 1 [PTK2]			0.651	indirect (22766276)	Y	x												x
1o1m_A	P69905	Hemoglobin alpha [HEMA]			0.651	none														
1euc_B	P53590	Succinyl-CoA synthetase beta [SCSB]			0.651	none														
1ram_A	Q04207	NF-kappa B p65 [NFKB]; negative control			0.576	none	Y				x	x	x	x			x			x

Supplementary Table S2. ILbind scores and kinetics that quantify interactions of CSA with calpain 2 (CAPN2), caspase 3 (CASP3), p38 mitogen-activated protein kinase 14 (MAPK14), cyclophilin A (positive control), and NF-kappa B p65 (NFKB; negative control). The measurements of kinetics were done in triplicate and we show the corresponding averages and standard deviations (stdev).

Target type	Target	ILbind score	average K_D ± stdev	average association rate ± stdev	average dissociation rate ± stdev
Positive control	Cyclophilin A	0.86	3.07E-08 ± 3.30E-08	2.53E+05 (fast) ± 3.29E+05	6.60E-03 (medium) ± 5.79E-03
Binding	CASP3	0.68	3.21E-04 ± 2.66E-04	2.36E+02 (slow) ± 2.8E+02	2.73E-02 (fast) ± 1.28E-02
Binding	CAPN2	0.67	3.22E-05 ± 5.56E-05	1.89E+04 (medium) ± 3.23E+04	1.86E-03 (medium) ± 3.16E-03
Binding	MAPK14	0.65	3.47E-05 ± 1.25E-05	4.01E+01 (slow) ± 5.63E+01	1.04E-03 (medium) ± 1.45E-03
Negative control	NFKB	0.58	N/A	N/A	N/A